Geostrophic Turbulence.

R. SALMON

Scripps Institution of Oceanography (A-025) - La Jolla, Calif., 92093

1. – Introduction.

Highly nonlinear, quasi-random motion in rapidly rotating, stably stratified fluid is called « geostrophic turbulence ». The subject has relevance to large-scale flow in the Earth's oceans and atmosphere. The theory of geostrophic turbulence bridges the distinct fields of geophysical fluid dynamics and statistical turbulence theory. The present lectures offer a self-contained but brisk introduction to both of these fields.

The quasi-geostrophic equations (sect. 2) form the basis for the theory. These equations approximate the general equations of fluid motion in the limit of small Rossby number. The Rossby number may be defined as the ratio of the Earth's rotation period (a day) to a characteristic time scale of the flow. The operative equation expresses the conservation of a scalar quantity called potential vorticity following fluid particles.

The quasi-geostrophic potential-vorticity equation generalizes the vorticity equation governing two-dimensional Navier-Stokes turbulence (sect. 3). The latter subject has aroused intense theoretical interest, in part for its geophysical relevance, but more perhaps for the opportunity it affords to test deductive theories of homogeneous turbulence against relatively high-resolution numerical experiments. Numerical simulations of three-dimensional turbulence are severely limited in spatial resolution by the computing capacity of even the most powerful modern machines.

The vast differences between two- and three-dimensional Navier-Stokes turbulence set the tone for our subject. The differences arise because vortex stretching, which is the primary mechanism of energy transfer from large to small scales of motion in three dimensions, is absent in two-dimensional flow. In two dimensions the simultaneous conservation of energy and vorticity actually implies a transfer of energy from the small to the large scales of motion. Simple arguments based upon energy and potential-vorticity conservation expose analogous distinctive properties of the quasi-geostrophic equations (sect. 4).

The complexity of turbulence invites statistical analysis. Classical statistical mechanics predicts the ideal states of « absolute equilibrium » towards which nonlinearities acting alone would drive the flow (sect. **5**). These states are strictly nonrealizable, but they indicate the qualitative role of nonlinear interactions in realistic, nonequilibrium flows. The quasi-geostrophic equilibrium states are unusual and instructive. For example, equilibrium nonequatorial flow is nearly depth-invariant at the largest scales of motion. Nonequilibrium (closure) theory is more complicated (sect. **6**), but has proved useful in conjunction with direct computer simulations of the equations of motion. Beta-plane turbulence (sect. **7**) is a case in point.

This is not a comprehensive review paper. Rather, topics were selected and ordered to illustrate the important ideas in logical sequence. The material in sect. **5** on « the equatorial funneling effect » is new.

2. – The quasi-geostropic equations.

We employ the quasi-geostrophic equations for a system comprised of two immiscible fluid layers with slightly different uniform densities (fig. 1). The upper surface at $z = n(x, y, t)$ is free and the lower rigid boundary lies at $z = -D + d(x, y)$, where $D = D_1 + D_2$, $D_i = \overline{h}_i$, $h_i(x, y, t)$ is the vertical thickness of the i-th fluid layer, and the overbar denotes horizontal average over the flow domain. The horizontal boundaries are rigid vertical walls or absent altogether.

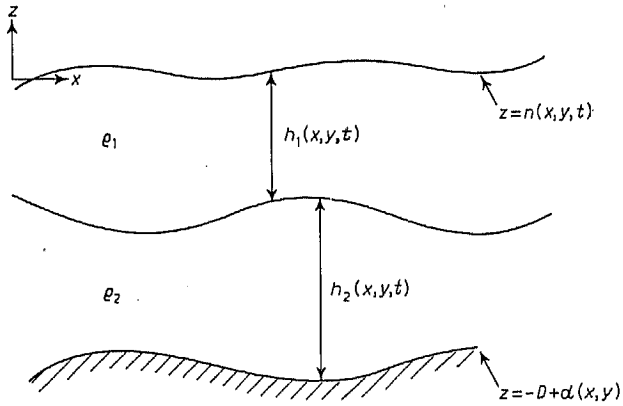

Fig. 1. – The geometry of the two-layer fluid.

Let $(L, U, L/U)$ be the scale for the (horizontal variability, horizontal velocity, time). If either

$$(D/L)^2 \ll 1 \quad \text{or} \quad R_0(D/L)^2 \ll 1 , \tag{2.1}$$

where $R_0 \equiv U/f_0 L$ is the « Rossby number », then the motion is hydrostatic, the horizontal velocity is depth-invariant within each layer, and the governing equations are the « shallow water » equations:

$$\frac{\partial \boldsymbol{u}_i}{\partial t} + \boldsymbol{u}_i \cdot \nabla \boldsymbol{u}_i + f\hat{k} \times \boldsymbol{u}_i = \begin{cases} -g\nabla n\,, & i = 1\,, \\ -g\nabla n + g'\nabla h_1\,, & i = 2\,, \end{cases} \tag{2.2}$$

and

$$\nabla \cdot \boldsymbol{u}_i + \frac{\partial w_i}{\partial z} = 0\,. \tag{2.3}$$

Here $\boldsymbol{u}_i = (u_i, v_i)$ is the horizontal and w_i the vertical velocity of the i-th layer, the (x, y, z) axis points (east, north, up), g is gravity, g' reduced gravity, and the Coriolis parameter

$$f = f_0 + \beta y\,, \tag{2.4}$$

where

$$f_0 = 2\Omega \sin \varphi_0\,, \qquad \beta = 2\Omega \cos \varphi_0 / r_E\,,$$

$\Omega = 2\pi$ day^{-1}, φ_0 is a reference latitude, and r_E is the radius of Earth. We assume $\bar{n} = 0$ and $|n| \ll h_i$. Then the vertical boundary conditions are

$$\begin{cases} w_1 = 0 & \text{at } z = 0\,, \\ w_i = -\left(\dfrac{\partial h_1}{\partial t} + \boldsymbol{u}_i \cdot \nabla h_1\right) & \text{at } z = -h_1 \end{cases} \tag{2.5}$$

and

$$w_2 = \boldsymbol{u}_2 \cdot \nabla d \qquad \text{at } z = -D + d\,.$$

Taking the vertical component of the curl $(\hat{k} \cdot \nabla \times\ )$ of (2.2) and using (2.3) yields the vorticity equations

$$\left(\frac{\partial}{\partial t} + \boldsymbol{u}_i \cdot \nabla\right)(\varrho_i + f) = (\varrho_i + f)\frac{\partial w_i}{\partial z}\,, \tag{2.6}$$

where

$$\varrho_i = \frac{\partial v_i}{\partial x} - \frac{\partial u_i}{\partial y} \tag{2.7}$$

is the relative vorticity. Integrate (2.6) through each layer and use (2.5). The result is

$$\left(\frac{\partial}{\partial t} + \boldsymbol{u}_i \cdot \nabla\right) q_i = 0\,, \tag{2.8}$$

where

$$q_i = (\varrho_i + f)/h_i \tag{2.9}$$

is the potential vorticity. In general, (2.8) is a single equation in the three dependent variables u_i, v_i and h_i. However, under the additional scaling assumptions of a rapid, slowly varying rotation rate,

$$R_0 \ll 1 \qquad \text{and} \qquad \beta L/f_0 \ll 1\,, \tag{2.10}$$

(2.8) reduces to an equation in a single unknown, and potential-vorticity conservation determines the full dynamics. The most convincing derivation is an expansion in powers of the Rossby number (see [1], p. 386). We shall be less formal. If (2.10) hold, then the horizontal momentum balance is geostrophic, that is, between the pressure gradient and Coriolis terms in (2.2). Thus

$$\boldsymbol{u}_i \approx \hat{k} \times \nabla \psi_i\,, \tag{2.11}$$

where

$$\psi_1 = gn/f_0 \tag{2.12}$$

and

$$\psi_2 = gn/f_0 - g' h_1/f_0\,. \tag{2.13}$$

Then

$$\varrho_i \approx \nabla^2 \psi_i\,, \tag{2.14}$$

$$h_1 \approx D_1 + f_0(\psi_1 - \psi_2)/g' \tag{2.15}$$

and

$$h_2 \approx D_2 + f_0(\psi_2 - \psi_1)/g' - d\,. \tag{2.16}$$

Substitution of (2.12)-(2.16) closes (2.8). But

$$|\varrho_i|/f_0 = O(R_0) \tag{2.17}$$

and

$$|\beta y|/f_0 = O(\beta L/f_0)\,, \tag{2.18}$$

which are both small parameters. If, in addition, we assume

$$|D_i - h_i|/D_i \ll 1\,, \tag{2.19}$$

then

$$q_i \approx \frac{f_0}{D_i}\left[1 + \frac{\varrho_i}{f_0} + \frac{\beta y}{f_0} + \frac{D_i - h_i}{D_i}\right] \tag{2.20}$$

and (2.8) reduces to the form used throughout these lectures:

$$\frac{\partial q_i}{\partial t} + J(\psi_i, q_i) = 0\,, \qquad J(A, B) \equiv \frac{\partial A}{\partial x}\frac{\partial B}{\partial y} - \frac{\partial B}{\partial x}\frac{\partial A}{\partial y}\,, \tag{2.21}$$

where

$$\begin{cases} q_1 = \nabla^2\psi_1 + F_1(\psi_2 - \psi_1) + f\,, \\ q_2 = \nabla^2\psi_2 + F_2(\psi_1 - \psi_2) + f + b(x, y)\,, \\ F_i \equiv f_0^2/g'D_i \qquad \text{and} \qquad b \equiv f_0 d/D_2\,. \end{cases} \tag{2.22}$$

The assumption of two immiscible fluid layers separated by a sharp change in density is appropriate for much of the ocean. However, (2.21), (2.22) are closely analogous to the corresponding equation for a continuously stratified fluid, *viz.*

$$\begin{cases} \dfrac{\partial q}{\partial t} + J(\psi, q) = 0\,, \\ q = \nabla^2\psi + \dfrac{\partial}{\partial z}\left(\dfrac{f^2}{\mathcal{N}^2}\dfrac{\partial \psi}{\partial z}\right) + f\,, \end{cases} \tag{2.23}$$

where $\mathcal{N}(z)$ is the buoyancy (or Väisälä) frequency. In particular (2.21), (2.22) are vertical-finite-difference analogs of (2.23). (See [1], p. 396.) Thus (2.21), (2.22) govern atmospheric motion as well. The rigid-lid condition (2.5*a*) becomes a crude model of the tropopause. More surprising is the fact that two vertical degrees of freedom appear adequate to resolve low-Rossby-number motions in both ocean and atmosphere. An explanation will be offered in sect. **4**. The parameters F_i in (2.22) may be specified in terms of the depth ratio

$$\Delta \equiv D_1/D_2 = F_2/F_1 \tag{2.24}$$

and the internal deformation radius

$$k_R^{-1} \equiv (F_1 + F_2)^{-\frac{1}{2}} \tag{2.25}$$

(units of length). Typical mid-latitude values are $\Delta = 1/7$, $k_R^{-1} = 50$ km for the ocean and $\Delta = 1$, $k_R^{-1} = 500$ km for the atmosphere. In these lectures we assume $\Delta = 1$ (for algebraic simplicity) corresponding to a linear mean density

gradient. Then

$$F_1 = F_2 = k_R^2/2 \,. \tag{2.26}$$

In simply connected geometry, the appropriate horizontal boundary conditions are $\psi_i = 0$. If islands are present, more general boundary conditions are required, but these are of no interest here.

In addition to potential vorticity, (2.21) conserves the total energy (proportional to)

$$\overline{\nabla\psi_1 \cdot \nabla\psi_1} + \overline{\nabla\psi_2 \cdot \nabla\psi_2} + k_R^2\overline{(\psi_1 - \psi_2)^2}/2 \,. \tag{2.27}$$

The terms in (2.27) represent the kinetic energy in the top layer, the kinetic energy in the bottom layer and the « available potential energy ». The latter vanishes when the interface is flat (cf. eqs. (2.15), (2.16)), which is the state of minimum potential energy. Currents with horizontal length scale L and order U shear across the interface have a ratio of available potential to kinetic energy of order $L^2k_R^2$, which can be very large. Such large-scale baroclinic currents exist and can be stable because of the rotation. Conversion from potential to kinetic energy is much less efficient in rotating than in nonrotating flow and takes the form of a « baroclinic instability » that prefers the length scale k_R^{-1}. Much of the special flavor of geophysical fluid dynamics derives from these facts. Linear stability theory offers a quantitative description in the small-amplitude regime, but more general arguments based on integral conservation properties alone lead qualitatively to the same results. The conservation arguments are valuable because they extend to realistic, nonlinear flow.

3. – Two-dimensional turbulence.

The vorticity equation for a single layer of uniformly rotating ($f = \text{const}$) Newtonian fluid over a flat bottom ($d = 0$) is

$$\frac{\partial\varrho}{\partial t} + J(\psi, \varrho) = \nu\nabla^2\varrho \,, \tag{3.1}$$

where

$$\varrho = \nabla^2\psi \,. \tag{3.2}$$

Two-dimensional turbulence governed by (3.1) is the prototype for geostrophic turbulence. Its distinctive property is a tendency for smaller eddies to feed their energy into the larger scales of motion [2, 3]. To isolate the role of nonlinear interactions specialize (3.1) to inviscid flow ($\nu = 0$). The inviscid equa-

tions conserve energy

$$\overline{\nabla\psi\cdot\nabla\psi} = \int_0^\infty \mathscr{E}(k, t)\,\mathrm{d}k\,, \tag{3.3}$$

and « enstrophy »

$$\overline{\varrho^2} = \int_0^\infty k^2\,\mathscr{E}(k, t)\,\mathrm{d}k\,, \tag{3.4}$$

where $\mathscr{E}(k, t)$ is the energy in wave number k (summed over all directions) at time t. Suppose $\mathscr{E}(k, 0)$ is concentrated at k_1 (fig. 2*A*)). If the energy subsequently spreads out to other wave numbers, then simultaneous conservation of the zeroth and second moments of $\mathscr{E}(k)$ implies that more energy moves

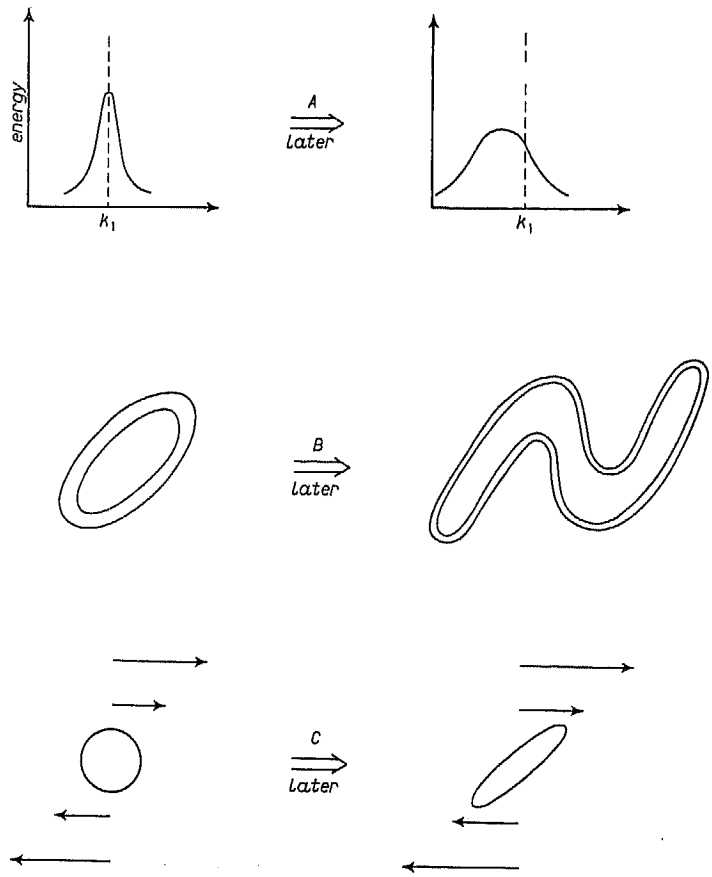

Fig. 2. – A trio of simple arguments illustrate the transfer of energy from small to large scales in two-dimensional flow.

toward wave numbers less than k than toward higher wave numbers. Precisely,

$$\frac{\mathrm{d}}{\mathrm{d}t}k_{\mathrm{E}} = -\frac{1}{2k_1}\frac{(\mathrm{d}/\mathrm{d}t)\int_0^\infty (k-k_1)^2\mathscr{E}(k,t)\,\mathrm{d}k}{\int_0^\infty \mathscr{E}(k)\,\mathrm{d}k}, \tag{3.5}$$

where

$$k_{\mathrm{E}} \equiv \int_0^\infty k\mathscr{E}(k,t)\,\mathrm{d}k \Big/ \int_0^\infty \mathscr{E}(k)\,\mathrm{d}k \tag{3.6}$$

is a wave number that characterizes the energy-containing scales of motion. The right side of (3.5) is negative if the dispersion of $\mathscr{E}(k)$ is increasing. By similar reasoning enstrophy moves chiefly to higher wave numbers. In three-dimensional turbulence, enstrophy is not conserved, and energy moves to high wave numbers.

The Fourier-space argument gives no hint at the mechanics of these transfers, but consider the following: If $\nu = 0$, then isolines of vorticity are also material lines, that is, always connect the same fluid particles. Consider two such neighboring lines of constant vorticity (fig. 2*B*)). If, as expected, these material lines lengthen on the average in time, then mass conservation requires their average separation to decrease, because the area between the lines is constant in two-dimensional flow. Thus the mean square vorticity gradient,

$$\overline{\nabla\varrho\cdot\nabla\varrho} = \int_0^\infty k^4\mathscr{E}(k,t)\,\mathrm{d}k\,, \tag{3.7}$$

increases, moving enstrophy into higher wave numbers.

Again, consider an initially isotropic small-scale eddy in a large-scale uniform shear (fig. 2*C*)). At a later time the eddy has been strained into the shape at the right, the Reynolds momentum flux $\overline{u_1'u_2'}$ is up the mean momentum gradient, and energy moves from the eddy into the mean flow. Crudely, if k is the wave number associated with the eddy and E is its energy, then, by vorticity conservation on particles, k^2E remains constant. But k increases as the eddy is stretched, and, therefore, E must decrease. The energy which is lost by the eddy must, by conservation of total energy, show up as an increase in the energy of the straining field.

Now consider the flow which develops when friction is restored and an external source injects energy continuously into the fluid at an intermediate wave number k_1. By all of the above arguments, we expect energy to move leftward (*i.e.* toward lower wave numbers) and enstrophy rightward from k_1.

Let ε_1 be the injection rate of energy (per unit mass per unit time) and n_1 the corresponding enstrophy injection rate. Let $\varepsilon(k)$ and $n(k)$ be the rates of nonlinear energy and enstrophy transfer past k (positive toward higher k). The viscosity in (3.1) is scale-selective. Let k_D be the highest wave number below which this viscosity is negligible. Then, if we assume quasi-steady statistics in the « inertial range » on $k_1 < k < k_D$, the nonlinear transfer of energy and enstrophy must be independent of k, *i.e.*

$$\varepsilon(k) = \varepsilon(k_D) \qquad \text{and} \qquad n(k) = n(k_D)\,. \tag{3.8}$$

Also

$$k_D^2\,\varepsilon(k_D) < n(k_D)\,, \tag{3.9}$$

by definition of k_D. Thus, if $\nu \to 0$ ($k_D \to \infty$), then $\varepsilon(k_D) \to 0$, since $n(k_D)$ cannot exceed n_1.

Inertial-range theory [4, 5] hypothesizes that, as $k_D/k_1 \to \infty$, the inertial range behaves like a « cascade » in which direct enstrophy transfer occurs only between eddies of comparable size. (Such transfer is also said to be « local » in wave number.) Towards the middle of the inertial range, which is many cascade steps removed from both forcing and viscosity, the energy spectrum depends plausibly only on k and $n = n(k)$. It then follows from dimensional requirements that

$$\mathscr{E}(k) = Cn^{2/3}k^{-3}, \qquad k_1 \ll k \ll k_D\,, \tag{3.10}$$

where C is a universal dimensionless constant. Similar arguments suggest the existence of an energy inertial range on $k \ll k_1$ in which $n(k)$ is zero, $\varepsilon = \varepsilon(k)$ is (a negative) constant,

$$\mathscr{E}(k) = C'|\varepsilon|^{2/3}k^{-5/3}, \qquad k \ll k_1\,, \tag{3.11}$$

and C' is another universal constant. Numerical experiments generally support these ranges [6], but the theoretical question of existence of « true » inertial ranges is both extremely thorny and probably irrelevant to the Earth's geophysical fluids. We regard (3.10) and (3.11) as conceptually useful idealizations.

There is a close correspondence between the k^{-1} enstrophy spectrum in the enstrophy-cascading inertial range and Batchelor's [7] k^{-1} spectrum for the variance of a passively advected scalar quantity. The passive scalar concentration obeys the same equation (3.1) as ϱ, but without (3.2). Batchelor's argument assumes only that the scales of motion contributing to the r.m.s.

strain rate σ are large compared to the length scales of scalar variability under consideration, and that the straining is persistent in time. If

$$\psi = \sigma x y \tag{3.12}$$

locally in the vicinity of $x = y = 0$, and the scalar field is a local sinusoid with wave number k, then, after a sufficient time,

$$\frac{\mathrm{d}k}{\mathrm{d}t} = \sigma k \tag{3.13}$$

following particles. Let $A(k)$ be the spectrum of scalar variance. The variance in a wave number band with initial width Δk centered on wave number k must, by conservation of variance, obey

$$A(k)\,\Delta k = A(\gamma k)\cdot(\gamma\,\Delta k)\,, \tag{3.14}$$

where $\gamma = \exp[\sigma t]$. The right side of (3.14) is the spectrum times the band width after time t. If the statistics are steady, then (3.14) holds for arbitrary γ. Thus

$$A(k) \propto k^{-1}. \tag{3.15}$$

Note that this argument does not require a localness-in-wave-number hypothesis (rather the opposite), so that Batchelor's theory might help explain why a k^{-3} energy spectrum is often observed when the conditions for a true inertial range seem lacking.

HALIKAS studied two-dimensional turbulence in a specially designed plexiglass tank on the rotating table at the Scripps Institution of Oceanography (plate 1). The tank radius and depth are comparable, so that the flow is two-dimensional only because the Rossby number is small. In a series of experiments, a vertical cylinder moving slowly relative to the tank released a column of dye in its wake. The dye streak (viewed from above) further demonstrates the dramatically different behavior of two- and three-dimensional turbulence. In nonrotating flow (plate 2), the dye sheet rapidly increases its surface area, molecular diffusion is very efficient, and the dye concentration quickly becomes uniform over a wide area. In rotating flow (plate 3), the fluid motion is columnar, the dye sheet increases its surface area much more slowly, and the dye remains concentrated in a small volume of fluid. Because of the vastly different dilution rates, Halikas' flow visualization technique actually works better in rotating than in nonrotating flow. This experiment is relevant to diffusion from a point source in the geophysical fluids.

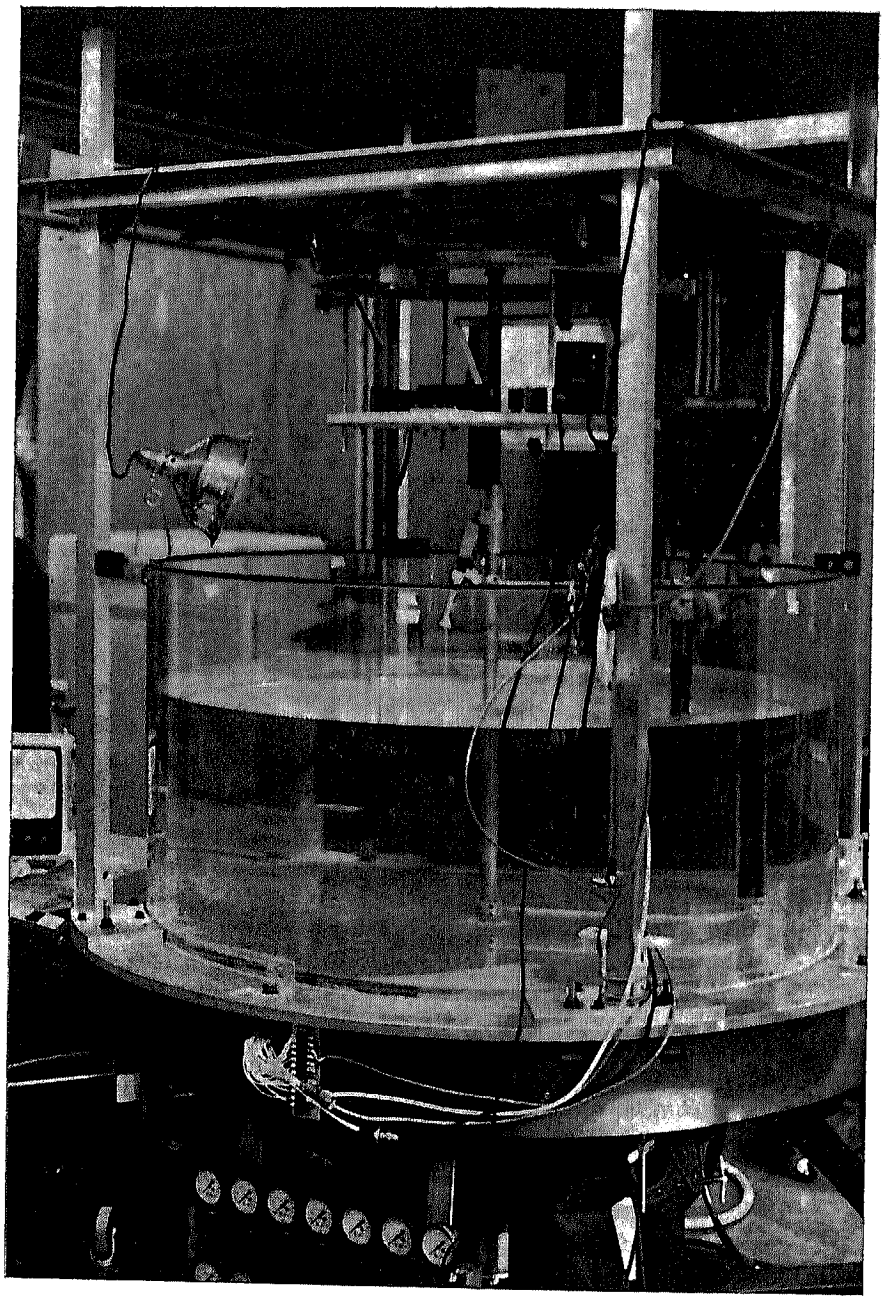

Plate 1. – Cylindrical tank on the rotating table. The vertical dye-filled column is moved by an arm attached to the axis of the tank. The tank diameter is 125 cm.

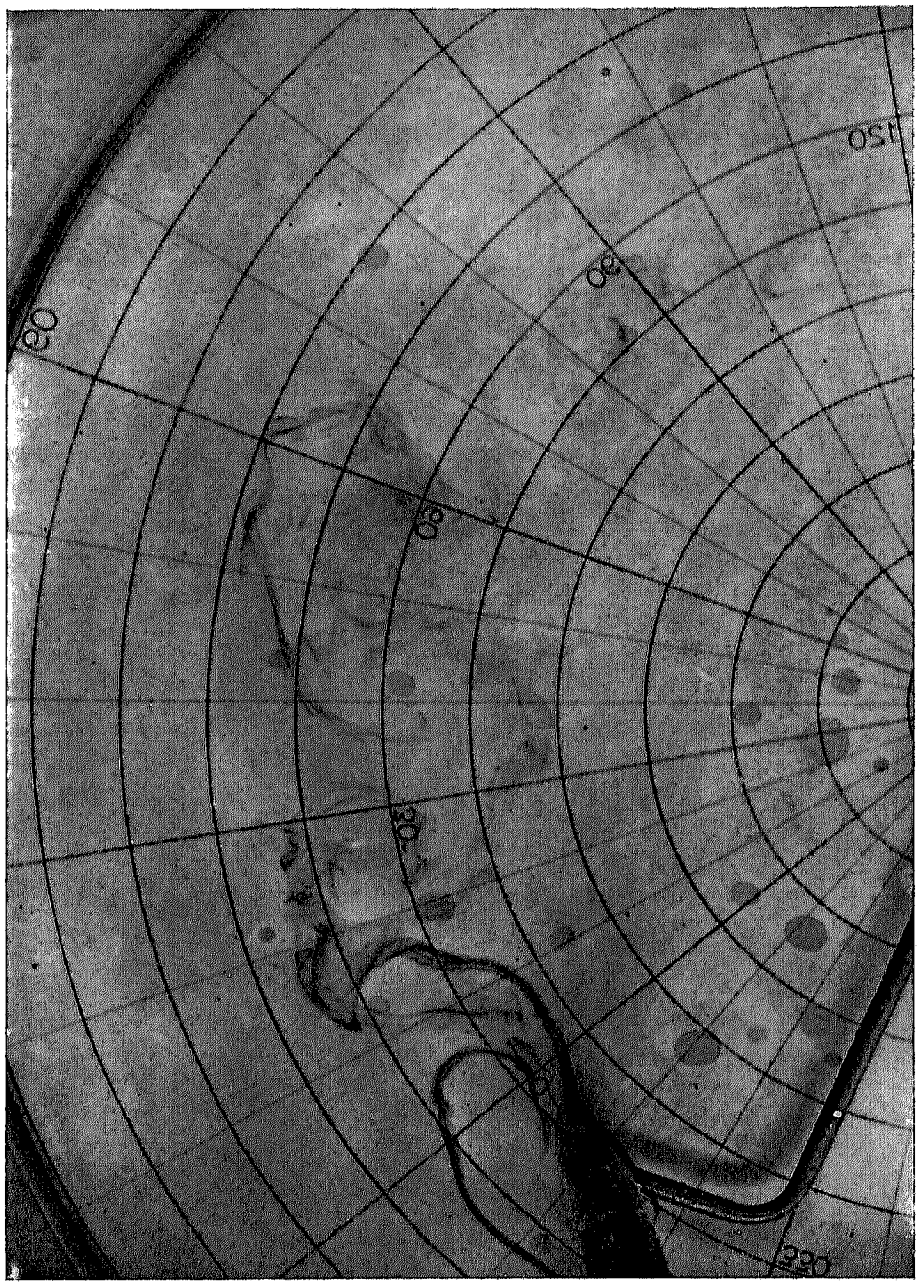

Plate 2. – Nonrotating flow. Towing period 78 s.

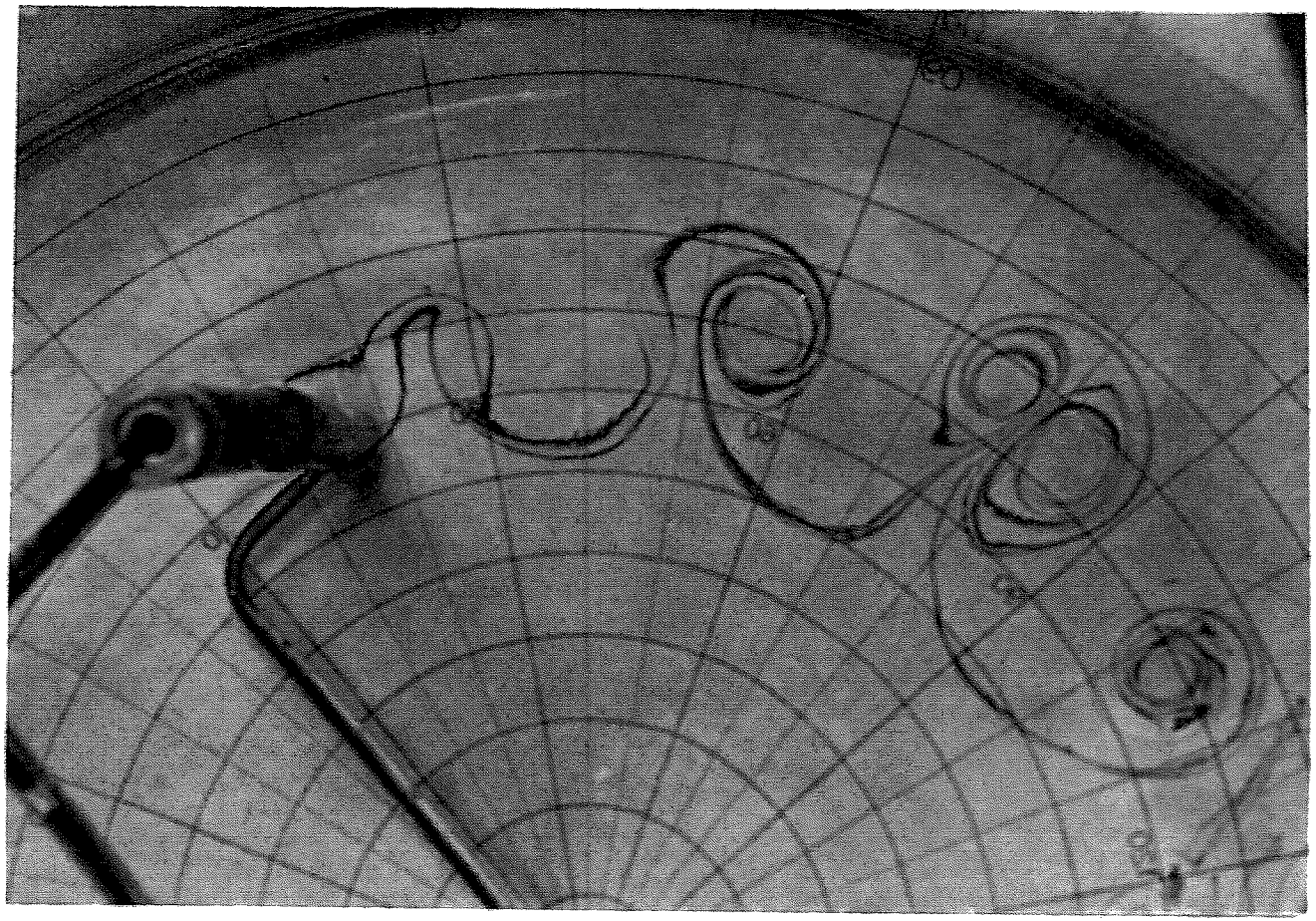

Plate 3. – Rotating flow. Towing period 7 s. Rotation period 3.55 s.

4. – Two-layer rotating turbulence.

The quasi-geostrophic equations (2.21), (2.22) for two-layer flow include the effects of density stratification, bottom topography and spatially variable rotation rate. The latter, particularly, has interesting consequences in the presence of horizontal boundaries. The remainder of these lectures will entertain each of these features in isolation. The present section treats horizontally unbounded stratified flow over a flat bottom [8-10]. The governing equations are (2.21), (2.22) with f constant, $D_1 = D_2$, and $b = 0$.

The discussion is simplest if we exchange ψ_1, ψ_2 for the vertical-mode variables

$$\psi = (\psi_1 + \psi_2)/2 \tag{4.1}$$

and

$$\tau = (\psi_1 - \psi_2)/2\,, \tag{4.2}$$

where ψ will be called the barotropic streamfunction and τ the baroclinic. Note that the upper thermocline displacement is proportional to

$$D_1 - h_1 = -2f_0\tau/g' \tag{4.3}$$

and that τ is temperaturelike in the sense that $\tau > 0$ implies a lower-than-average vertically averaged density. The (inviscid) dynamics become

$$\frac{\partial}{\partial t}\nabla^2\psi + J(\psi, \nabla^2\psi) + J(\tau, \nabla^2\tau) = 0 \tag{4.4}$$

and

$$\frac{\partial}{\partial t}\nabla^2\tau + J(\psi, \nabla^2\tau) + J(\tau, \nabla^2\psi) = k_{\mathrm{R}}^2\left[\frac{\partial\tau}{\partial t} + J(\psi, \tau)\right]. \tag{4.5}$$

Let the streamfunctions be expanded in Fourier series:

$$(\psi, \tau) = \sum_{\boldsymbol{k}} (\psi_{\boldsymbol{k}}, \tau_{\boldsymbol{k}}) \exp[i\boldsymbol{k}\cdot\boldsymbol{x}]\,, \tag{4.6}$$

and define

$$U(\boldsymbol{k}) = k^2|\psi_{\boldsymbol{k}}|^2 \qquad \text{and} \qquad E(\boldsymbol{k}) = (k^2 + k_{\mathrm{R}}^2)|\tau_{\boldsymbol{k}}|^2. \tag{4.7}$$

We call $U(\boldsymbol{k})$ the barotropic energy in wave number $\boldsymbol{k}$ and $E(\boldsymbol{k})$ the total baroclinic energy. The latter consists of baroclinic kinetic energy and available potential energy in the ratio k^2/k_{R}^2.

The quadratic integral invariants of the motion are the total energy and the potential enstrophy $\overline{q_i^2}$ of each layer. It is convenient to replace the latter two by their sum and difference, which are, of course, also conserved. Then conservation of the energy and sum enstrophy are equivalent to

$$\frac{\mathrm{d}}{\mathrm{d}t}\sum_{\boldsymbol{k}}[U(\boldsymbol{k})+E(\boldsymbol{k})]=0 \tag{4.8}$$

and

$$\frac{\mathrm{d}}{\mathrm{d}t}\sum_{\boldsymbol{k}}[k^2U(\boldsymbol{k})+(k^2+k_{\mathrm{R}}^2)E(\boldsymbol{k})]=0\,. \tag{4.9}$$

Conservation of the difference potential enstrophy,

$$\sum_{\boldsymbol{k}}k^2(k^2+k_{\mathrm{R}}^2)\psi_{\boldsymbol{k}}\tau_{-\boldsymbol{k}}\,, \tag{4.10}$$

puts a restriction on energy transfer between layers. However, our arguments require only (4.8) and (4.9). The analogy with two-dimensional turbulence is already apparent. The energies enter (4.8), (4.9) precisely as in two-dimensional turbulence, except that the baroclinic energy $E(\boldsymbol{k})$ has an effective square wave number of $k^2+k_{\mathrm{R}}^2$. By analogy with two-dimensional turbulence, we expect the total energy to move toward lower effective wave numbers. Thus (4.8) and (4.9) imply that nonlinear interactions barotropize the flow.

The quadratic integral invariants of the motion are significant because they are conserved by individual wave number triads. Let $\boldsymbol{k}$, $\boldsymbol{p}$, $\boldsymbol{q}$ be any three horizontal wave numbers that sum vectorially to zero:

$$\boldsymbol{k}+\boldsymbol{p}+\boldsymbol{q}=0\,. \tag{4.11}$$

The dynamics permits two types of triad in the two-layer fluid. One type consists of three barotropic components and the other consists of one barotropic and two baroclinic components. Energy transfer in the two types of triad is constrained by the detailed forms of (4.8) and (4.9), namely

$$\begin{cases}\dot{U}(\boldsymbol{k})+\dot{U}(\boldsymbol{p})+\dot{U}(\boldsymbol{q})=0\,,\\ k^2\dot{U}(\boldsymbol{k})+p^2\dot{U}(\boldsymbol{p})+q^2\dot{U}(\boldsymbol{q})=0\,,\end{cases} \tag{4.12}$$

and

$$\begin{cases}\dot{U}(\boldsymbol{k})+\dot{E}(\boldsymbol{p})+\dot{E}(\boldsymbol{q})=0\,,\\ k^2\dot{U}(\boldsymbol{k})+(p^2+k_{\mathrm{R}}^2)\dot{E}(\boldsymbol{p})+(q^2+k_{\mathrm{R}}^2)\dot{E}(\boldsymbol{q})=0\,,\end{cases} \tag{4.13}$$

where the tendencies in (4.12), (4.13) are those resulting from interactions with other members in the triad. (Thus $\dot{U}(\boldsymbol{k})$ is different in (4.12) and (4.13).)

The constraints (4.12) on the UUU triad are the same as in two-dimensional turbulence. In (4.12) suppose $k \leqslant p \leqslant q$. The constraints (4.12) prevent energy transfer between different scales of motion in both extremely local ($k \approx p$) and extremely nonlocal ($k \ll p$) triads. In three-dimensional turbulence only (4.12a) holds and any shape triad can transfer energy between scales.

For UEE triads the deformation radius is a critical length scale. When $k, p, q \gg k_{\mathrm{R}}$ the constraints (4.13) are the same as (4.12), so that energy transfer in the UEE triads is the same as in two-dimensional turbulence. This agrees with the physical picture of two-layer flow on scales smaller than the deformation radius as being essentially uncoupled single layers which see the interface as a rigid boundary. However, the situation when $k, p, q \ll k_{\mathrm{R}}$ is similar to three-dimensional turbulence. In this case energy transfer is between the two baroclinic components only and may be either local ($p = O(q)$) or nonlocal ($p \ll q$). Because of k_{R} in (4.13b), the enstrophy constraint poses no inhibition against rightward transfer of baroclinic energy on wave numbers less than k_{R}. If $k = O(k_{\mathrm{R}})$ in (4.13), then energy can be transferred to the barotropic component $U(\boldsymbol{k})$ as well.

An extension of the above ideas yields the direction of wave number energy transfer in forced-equilibrium flow. Consider a hypothetical two-layer fluid with a minimum wave number $k_0 \ll k_{\mathrm{R}}$ near which stirring and/or heating forces act. « Dissipation » is also present, but, for simplicity, it is limited to only two regions of the spectrum: near k_0, where it models the loss of large-scale energy to (Ekman-type) frictional boundary layers, and near $k_{\mathrm{D}} \gg k_{\mathrm{R}}$, where it parameterizes the transition from two- to three-dimensional flow on scales too small to feel the Earth's rotation. In the general inertial region $k_0 < k < k_{\mathrm{D}}$ neither forcing nor dissipation is significant. The fluid is assumed to reach a statistically steady state in which the transfer of total energy and sum enstrophy past k is the same for every k on $k_0 < k < k_{\mathrm{D}}$. On scales smaller than the deformation radius, the dynamics are those of uncoupled single layers in which the general invariants reduce to ordinary kinetic energy and enstrophy. Since the only energy source is at k_0, we expect k^{-3} enstrophy inertial ranges on $k_{\mathrm{R}} < k < k_{\mathrm{D}}$. If $k_{\mathrm{D}}/k_{\mathrm{R}}$ is large, then the energy reaching k_{D} is negligible. This means that the large scales must adjust to a state in which the net energy production at k_0 is zero, that is

$$\dot{U}(\boldsymbol{k}_0)_{\mathrm{nc}} + \dot{E}(\boldsymbol{k}_0)_{\mathrm{nc}} = 0\,, \tag{4.14}$$

where the subscripts nc denote tendencies due to forcing and dissipation. Because of (4.14) the potential-enstrophy production is proportional to

$$k_{\mathrm{R}}^2 \dot{E}(\boldsymbol{k}_0)_{\mathrm{nc}}\,. \tag{4.15}$$

The potential-enstrophy production equals the transfer rate of potential enstrophy across $k_0 < k < k_D$, and it must be positive since there is only an enstrophy sink at k_D. Thus (4.15) is positive, $\dot{U}(\boldsymbol{k}_0)_{nc}$ must be negative by (4.14), and internal interactions must transfer large-scale energy from baroclinic to barotropic mode. However, by the reasoning given above, large-scale baroclinic components can transfer energy only between themselves. The transfer from baroclinic to barotropic mode must, therefore, occur on $k_0 < k < k_R$ as a rightward transfer of baroclinic energy in *UEE* triads and an equal and opposite leftward transfer of barotropic energy in *UUU* triads. The conversion of baroclinic to barotropic energy can occur near k_R. Figure 3 summarizes the energy flow in wave number space. Potential-enstrophy transfer, which may be deduced by similar arguments, is indicated by dashed arrows. Figure 3 differs from the wave number energy flow diagrams conventionally drawn in meteorology in that both the upper horizontal and vertical arrows represent a conversion of potential to kinetic energy.

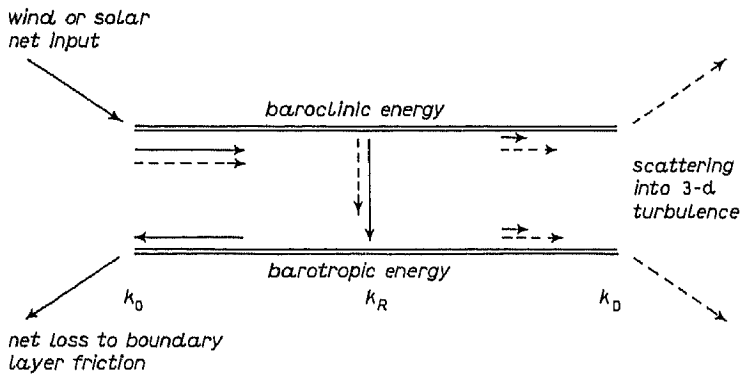

Fig. 3. – The wave number energy flow diagram for a two-layer system. The solid arrows represent energy flow and the dashed arrows sum potential-enstrophy flow.

The generalization of these ideas to multilayer or continuously stratified flow is straightforward. The multilayer system conserves

$$\int_0^\infty [E_0(k) + E_1(k) + E_2(k) + \ldots]\,\mathrm{d}k \tag{4.16}$$

and

$$\int_0^\infty [k^2 E_0(k) + (k^2 + k_1^2) E_1(k) + (k^2 + k_2^2) E_2(k) + \ldots]\,\mathrm{d}k\,, \tag{4.17}$$

where $E_n(k)$ is the energy in horizontal wave number k and vertical mode n, k_n^{-1} is the n-th internal deformation radius, and $k_1 = k_R$. In a uniformly

stratified ocean,

$$k_n = n\pi f/\mathcal{N}D\,. \tag{4.18}$$

We expect net energy transfer into modes (k, n) with lower total wave numbers $k^2 + k_n^2$. But k_n increases with n. Observations do indeed suggest that the barotropic $(n = 0)$ and first baroclinic $(n = 1)$ modes hold most of the energy in nonequatorial geostrophic flow [11].

Now consider what happens as k_n varies with latitude through its dependence on f. As the equator is approached, the k_n vanish, removing the inhibition against high vertical-mode numbers. Since the total wave number $\sqrt{k^2 + k_n^2}$ of each mode (k, n) is smaller than its value in mid-latitudes, the total energy at the equator will be greater than in mid-latitude. Thus the same logic that predicts negative eddy viscosity in two dimensions suggests that a uniformly excited ocean would transfer energy equatorward and into high vertical wave numbers. Recent observations of the equatorial ocean reveal that the equator does contain a surprising amount of low-frequency energy in high vertical wave numbers [12]. These large-amplitude equatorial motions have previously been explained as a forced response to local winds [13]. The above arguments suggest, however, that energy at higher latitudes could be the source for equatorial motion. However, the quasi-geostrophic approximation itself breaks down at the equator, so that these ideas require some generalization. We shall return to this « equatorial funneling effect » in the following section.

5. – Entropy and absolute equilibrium.

Classical statistical mechanics can apply to the macroscopic motions of ideal fluids and other continuous fields [2, 14, 15]. The macroscopic analog of thermal equilibrium is physically nonrealizable, but it anticipates the role played by nonlinear interactions in realistic nonequilibrium flow. We commence with a swift review of the basics, adopting the information theory viewpoint [16]. This approach emphasizes the guessing nature of the whole subject.

Consider a general mechanical system whose precise state is specified by the value of N real numbers $[y_1, y_2, \ldots, y_N]$ and whose dynamics is governed by N first-order ordinary differential equations of the form

$$\dot{y}_i = G_i(y_1, y_2, \ldots, y_N)\,. \tag{5.1}$$

This form encompasses our fluid equations if $N = \infty$. For example, let the y_i be defined by

$$\psi = \sum_i (y_i/k_i)\,\varphi_i(\boldsymbol{x})\,, \tag{5.2}$$

where $\varphi_i(\boldsymbol{x})$ is a normalized eigenfunction satisfying

$$\nabla^2\varphi_i + k_i^2\varphi_i = 0\,, \qquad \overline{\varphi_i^2} = 1\,, \tag{5.3}$$

and $\varphi_i = 0$ on the boundary of the fluid, and k_i^2 is the associated eigenvalue. Then (3.1) transforms to

$$\dot{y}_i = \sum_{j,l} A_{ijl} y_j y_l - \nu_i y_i\,, \tag{5.4}$$

where

$$A_{ijl} = (k_j/k_i k_l)\,\overline{\varphi_i J(\varphi_l, \varphi_j)} \tag{5.5}$$

and

$$\nu_i = \nu k_i^2\,. \tag{5.6}$$

The N-dimensional space spanned by the y_i is called phase space, and each point in phase space represents a possible state of the system as a whole. Every realization of (5.4) traces out a trajectory in phase space.

Let the joint-probability distribution of the y_i in an ensemble of realizations of (5.4) be

$$P(y_1, y_2, \ldots, y_N, t)\,. \tag{5.7}$$

Since the moving phase points that represent individual realizations of (5.4) can neither be created nor destroyed,

$$\frac{\partial P}{\partial t} + \sum_i \frac{\partial}{\partial y_i}(\dot{y}_i P) = 0\,, \tag{5.8}$$

where $\dot{y}_i$ is given by (5.4). Equation (5.8) is analagous to the continuity equation in fluid mechanics with P (the density of phase points) replacing the ordinary fluid density, $\dot{y}_i$ (the i-direction velocity of phase points) replacing the fluid velocity, and the summation over N phase-space dimensions replacing the summation over three physical-space dimensions. If (5.4) is such that

$$\sum_i \partial\dot{y}_i/\partial y_i = 0\,, \tag{5.9}$$

then (5.8) reduces to

$$\frac{\partial P}{\partial t} + \sum_i \dot{y}_i \frac{\partial P}{\partial y_i} = 0\,, \tag{5.10}$$

which is the analog of the continuity equation for an incompressible fluid. Hamiltonian systems satisfy (5.9) automatically provided that the y_i are chosen to be generalized co-ordinates and momenta. For the fluid systems considered

here, (5.9) holds because A_{ijl} vanishes whenever two of its indices are equal. (The fluid equations can, in fact, be derived from Hamilton's principle (see, for example [17], p. 3). However, a close connection between the corresponding canonical equations (which involve functional derivatives) and (5.9) has not been demonstrated. In practice, it seems easiest to verify (5.9) directly as needed.)

Equation (5.10) implies that the volume occupied by a collection of phase particles always containing the same particles remains constant in time. This contraint, while important, is not confining. Consider, for example, a two-dimensional phase space in which P is initially constant within a compact region and zero outside (fig. 4). In a wide class of physical systems, which are

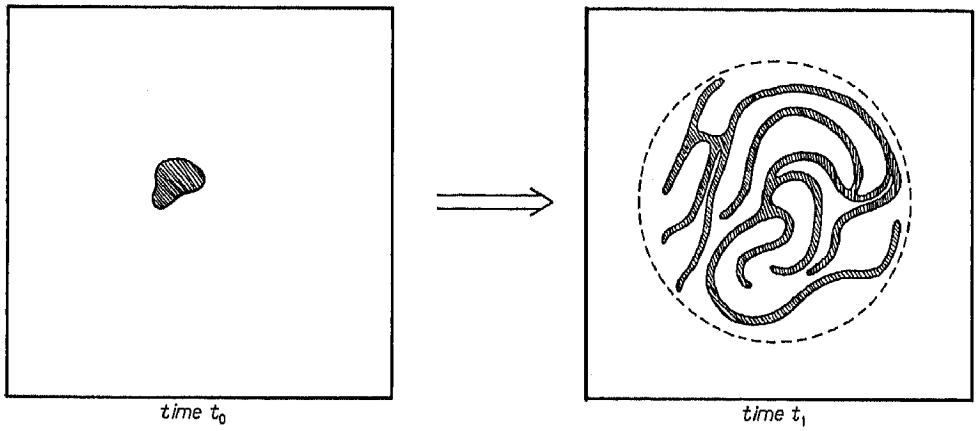

Fig. 4. – Mixing in a two-dimensional phase space.

said to « mix », the initially compact region « spreads out » by developing filamentous arms which gradually « fill up » the phase space. Now P is typically sought for computing the statical average of phase functions $F(y_1, y_2, \ldots, \ldots, y_N, t)$, *viz.*

$$\langle F \rangle = \int\int \ldots \int F P \prod_i \mathrm{d}y_i \,. \tag{5.11}$$

Suppose that P does indeed evolve from time t_0 to t_1, as shown in fig. 4. In practice, it is usually impossible to calculate $P(t_1)$ accurately from (5.10) for use in (5.11). However, it is obvious that, for any F that depends smoothly on its arguments, $\langle F \rangle$ at t_1 can be calculated to good accuracy by replacing $P(t_1)$ with a density function that is constant over the circular region of fig. 4. We, therefore, distinguish between $P(t)$, the probability density obtained from (5.10) by solution of (5.4) for a entire ensemble of systems, and $\hat{P}(t)$, the « phenomenological » or practical density, which can be considered a smooth-

ed version of $P(t)$. Statistical mechanics seeks $\hat{P}(t)$ without first calculating $P(t)$. The mixing property of the dynamics motivates the concept of $\hat{P}(t)$, but it also imposes the consistency requirement that $\hat{P}(t)$ ought to be progressively more «spread out» at successively later times. This is a qualitative statement of the second law.

Entropy is a functional of $\hat{P}$ which measures the spread of $\hat{P}$, that is, by how much $\hat{P}$ differs from a delta-function in phase space. If the y_i can assume only discrete values y_{ii}, then the entropy takes the form

$$S = -\sum_i \sum_i \hat{P}_{ii} \ln \hat{P}_{ii} \tag{5.12}$$

([18], p. 9). If the y_i assume continuous values, then (5.12) generalizes to

$$S = -\int\int \ldots \int \hat{P} \ln \hat{P} \cdot \mathscr{M} \prod_i \mathrm{d}y_i , \tag{5.13}$$

where $\mathscr{M}$ is an undetermined measure of the phase space. Because of (5.9), however, $\mathscr{M}$ must be a constant. To see this, specialize to the inviscid case and imagine an extremely clever observer for whom integration of (5.4), (5.10) presents no difficulty. For such an observer, $P = \hat{P}$ at all times, and the entropy should not increase. However, (5.10) implies that

$$\int\int \ldots \int P \ln P \cdot \mathscr{M} \prod_i \mathrm{d}y_i \tag{5.14}$$

can remain constant only if $\mathscr{M}$ is a constant.

Practical knowledge about a mixing system based upon partial (*i.e.* statistical) specification of its initial state always decreases in time, and the entropy, therefore, increases. However, information about quantities which are constants of the motion is never degraded in time. Absolute equilibrium is defined to be the state in which only certain integral constants of the motion are known. (Only linear and quadratic invariants are easily handled. However, these seem to be the most important.) Unfortunately, if $\nu \neq 0$, then (5.4) has no constants of the motion. Viscous ensembles cannot, therefore, approach absolute equilibrium. However, if the «mixing time» is short compared to the viscous time for at least a subset of phase co-ordinates, then qualitative features of absolute equilibrium can appear in realistic, dissipative flows.

We begin by calculating absolute equilibrium for two-dimensional turbulence. The constants of the motion are the energy

$$E = \sum_i E_i \equiv \sum_i y_i^2 \tag{5.15}$$

and the enstrophy

$$\Omega = \sum_i \Omega_i \equiv \sum_i k_i^2 y_i^2 . \tag{5.16}$$

To discover $\hat{P}$, maximize S subject to the requirements

$$\langle 1 \rangle = 1 , \qquad \langle E \rangle = E_0 , \qquad \langle \Omega \rangle = \Omega_0 , \tag{5.17}$$

where E_0 and Ω_0 are known initial values. The result is

$$\hat{P} = \exp[\lambda - \alpha E - \gamma \Omega] , \tag{5.18}$$

where λ, α, γ are constants determined from (5.17). Directly from (5.18)

$$\langle y_i^2 \rangle = \tfrac{1}{2}(\alpha + \gamma k_i^2)^{-1}, \tag{5.19}$$

which shows that the quantity $\alpha E_i + \gamma \Omega_i$ is equipartitioned among the modes. Equation (5.19) implies an energy spectrum proportional to

$$k/(\alpha + \gamma k^2) , \tag{5.20}$$

which corresponds to infinite total energy and enstrophy, because the integral of (5.20) diverges at large wave number. In three dimensions energy alone is equipartitioned, the equilibrium spectrum goes like k^2, and the divergence is even more catastrophic. These equilibrium states are, therefore, realizable only if the system is artificially truncated to finite N, as if, for example, all modes with wave numbers larger than some arbitrarily chosen cut-off k_c were excluded from the dynamics. The truncated system still satisfies (5.9). A thought experiment in which k_c is raised by finite increments, with the system allowed to re-equilibrate at each new value of k_c, then suggests that nonlinear interactions in three-dimensional turbulence would, acting by themselves, pass all of the energy out to infinite wave number. This conclusion seems rather tame, but similarly spirited interpretations of the formally divergent equilibrium states corresponding to more complicated dynamics yield useful and sometimes surprising predictions [19].

Consider, for example, the flow of a single layer of rotating fluid over topography. The dynamics are

$$\frac{\partial q}{\partial t} + J(\psi, q) = 0 , \tag{5.21}$$

where

$$q = \nabla^2 \psi + h(x, y) \tag{5.22}$$

and

$$h = f(y) + b(x, y)\,. \tag{5.23}$$

The notation is the same as in sect. **2**. In terms of the coefficients y_i defined by (5.2), the quadratic invariants are the energy,

$$E = \sum_i y_i^2\,, \tag{5.24}$$

and the potential enstrophy (less a constant),

$$\Omega = \sum_i k_i^2 y_i^2 - 2\sum_i k_i h_i\,. \tag{5.25}$$

Again the equilibrium state is multivariate Gaussian, but now there is a non-zero mean flow,

$$\langle y_i\rangle = \gamma k_i h_i/(\alpha + \gamma k_i^2)\,, \tag{5.26}$$

which is locked to the topography. The energy in mode i,

$$\langle y_i^2\rangle = \tfrac{1}{2}(\alpha + \gamma k_i^2)^{-1} + \langle y_i\rangle^2, \tag{5.27}$$

is enhanced by the energy in the average contour current. The transform of (5.26),

$$\left(\frac{\alpha}{\gamma} - \nabla^2\right)\langle\psi\rangle = h\,, \tag{5.28}$$

is useful if $h(x, y)$ has coherent form. Note that $\langle\psi\rangle$ is an exact steady solution to (5.21), (5.22).

If the nonlinear terms in (5.21) are suppressed, then the enstrophy invariant reduces to $\overline{h\nabla^2\psi}$, the mean flow vanishes if the latter is initially zero, and absolute equilibrium has energy equipartition. The topography scatters energy into higher wave numbers, but the linear dynamics prevents vortex stretching on slopes from accumulating vorticity of preferred sign on topographic peaks and troughs.

Numerical simulation of (5.21) with random topography and constant f confirm all of these qualitative predictions [20]. Figure 5 shows the enstrophy spectrum after 2.5 turn-over times in three independent experiments with identical, sharply peaked initial spectra. The three experiments correspond to *a*) no topography (long dashes), *b*) topography and nonlinearity of equal strength (solid line) and *c*) no nonlinearity (short dashes). The topography spectrum is hatched. The induced mean flow in case *b*) shows up as a spectral

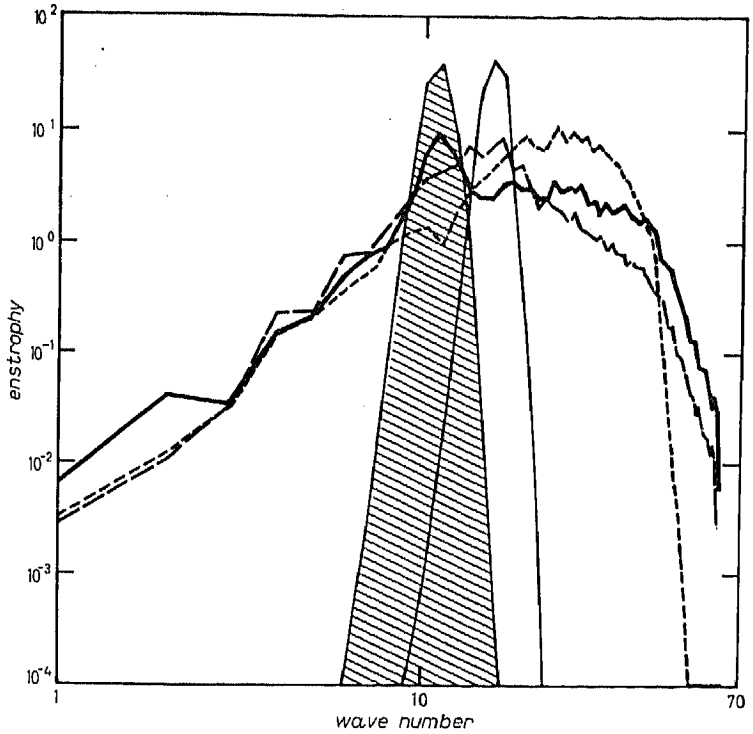

Fig. 5. – Enstrophy spectra of two-dimensional turbulence over topography after 2.5 turn-overs beginning from a narrow spectral peak. The three experiments correspond to no topography (long dashes, $R_0/\delta = \infty$), topography and nonlinearity of equal strength (solid, $R_0/\delta \approx 1$) and no nonlinearity (short dashes, $R_0/\delta \simeq 0$). The topography spectrum is hatched. Courtesy of G. HOLLOWAY.

bump at the topography wave numbers and as a visually apparent correlation between the topography and instantaneous streamfunction (fig. 6). Topographic scattering increases the enstrophy at high wave numbers in both cases *b*) and *c*), but more so in *c*), where the enstrophy transfer to high wave numbers is not linked to energy transfer to low wave numbers by an enstrophy invariant.

An interesting special case of (5.21), (5.22) is beta-plane flow in a rectangular flat-bottomed ocean, $0 < x < L$, $0 < y < L$. The mean-flow equation is

$$\left(\frac{\alpha}{\gamma} - \nabla^2\right)\langle\psi\rangle = \beta(y - y_0) \tag{5.29}$$

with $\langle\psi\rangle = 0$ on boundaries. The constants α, γ are determined from

$$E_0 = \langle E\rangle = \tfrac{1}{2}\sum_i (\alpha + \gamma k_i^2)^{-1} + \overline{\nabla\langle\psi\rangle\cdot\nabla\langle\psi\rangle} \tag{5.30}$$

and

$$\Omega_0 = \langle \Omega \rangle = \tfrac{1}{2} \sum_i k_i^2 (\alpha + \gamma k_i^2)^{-1} + \overline{\langle \nabla^2 \psi \rangle}^2 + 2f \overline{\langle \nabla^2 \psi \rangle} \,, \tag{5.31}$$

where E_0 and Ω_0 are the initial energy and enstrophy. (The constant y_0 can be considered a Lagrange multiplier corresponding to a third possible integral invariant, the average potential vorticity $\bar{q}$.) Let the initial state be a random field concentrated at wave number $k_* = O(L^{-1})$ and uncorrelated with latitude. Then $\Omega_0 = k_*^2 E_0$ and the initial Rossby number is small if $E_0 \ll \beta^2 L^4$.

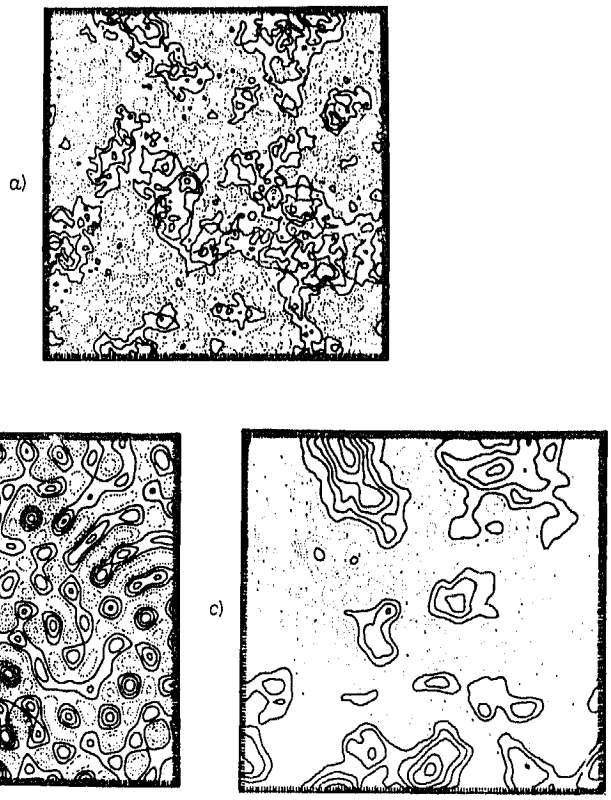

Fig. 6. – The topography (a)), initial streamfunction (b)) and the streamfunction after four turn-overs (c)). Courtesy of G. HOLLOWAY.

The equilibrium mean flow exceeds the initial bounds on energy or enstrophy unless

$$0 < \frac{\gamma}{\alpha} \equiv l^2 \ll L^2 \,. \tag{5.32}$$

Thus consistent solutions to (5.29) have a westward interior flow with speed βl^2 and boundary layers of thickness l and characteristic speed $\beta L l$. The total mean kinetic energy is shared equally by the boundary layers and the interior flow, but the boundary layers constitute the sole contribution of the mean flow to the enstrophy. This mean flow is the same as that derived by FOFONOFF [21] in another context. The transient energy is spread uniformly throughout the basin and the transient spectrum has a (broad) peak at wave number l^{-1}. Thus the eddies have the same scale as the boundary layer thickness and cannot grow larger without breaking the constraints. Note that the scale l is unrelated to the deformation radius. This small-scale energy originates from Rossby-wave reflection at the western boundary [22].

Multilayer equilibria show how energy gets spread among the vertical modes. For example, absolute equilibrium for the two-layer system with equal layer depths and the same initial energy spectrum in each layer has barotropic energy

$$U(\boldsymbol{k}) = 1/(\alpha + \gamma k^2) \tag{5.33}$$

and baroclinic energy

$$E(\boldsymbol{k}) = 1/[\alpha + \gamma(k^2 + k_R^2)] . \tag{5.34}$$

Thus

$$E(k) = U(\sqrt{k^2 + k_R^2}) . \tag{5.35}$$

In all cases of interest, the equilibrium $U(k)$ increases with decreasing k. Thus the equilibrium flow is nearly barotropic on scales larger than the deformation radius. Paradoxically, then, depth-invariant flow constitues the « most disordered » state for large-scale ocean currents. Strong barotropic flows are in fact observed. RHINES [23] describes a six-month mooring record in which a transient 20 cm/s current remained nearly depth-invariant through 4000 m depth over the entire observing period. The site was in the energetic Gulf Stream extension region, over a smooth abyssal plain. The generalization of (5.33), (5.34) to a N-layer system is

$$E_n(\boldsymbol{k}) = 1/[\alpha + \gamma(k^2 + k_n^2)] , \tag{5.36}$$

where k_n is given by (4.18). The higher vertical modes contain decreasing amounts of energy in equilibrium.

We next consider absolute equilibria for flows with variable Väisälä frequency and Coriolis parameter. These equilibria suggest how far the previously postulated « equatorial funneling effect » would proceed. Because $\mathcal{N}(z)$ and $f(y)$ are spatially inhomogeneous, it is now more natural to formulate the problem in physical space than in transform space. First, consider continuous

stratification. The dynamics are

$$\frac{\partial q}{\partial t} + J(\psi, q) = 0 \,, \tag{5.37}$$

where

$$q = \mathscr{L}[\psi] + f(y) \tag{5.38}$$

and

$$\mathscr{L}[\psi] = \nabla^2 \psi + \frac{\partial}{\partial z}\left[\frac{f^2}{\mathscr{N}^2}\frac{\partial \psi}{\partial z}\right]. \tag{5.39}$$

The boundary conditions are

$$\partial\psi/\partial z = 0 \qquad \text{at } z = 0, -D \,, \tag{5.40}$$

corresponding to zero vertical velocity. It is temporarily convenient to expand ψ and q in the eigenmodes $\varphi_i(x, y, z)$ of the operator $\mathscr{L}$. These obey

$$\mathscr{L}[\varphi_i] + \lambda_i^2 \varphi_i = 0 \tag{5.41}$$

and

$$\frac{\partial \varphi_i}{\partial z} = 0 \qquad \text{at } z = 0, -D \,, \tag{5.42}$$

where i is the index for the eigenmodes and λ_i^2 is the corresponding eigenvalue. Then, if

$$\psi = \sum_i a_i \varphi_i \qquad \text{and} \qquad f = \sum_i f_i \varphi_i \,, \tag{5.43}$$

it follows from (5.39) that

$$q = \sum_i (-\lambda_i^2 a_i + f_i)\varphi_i \,. \tag{5.44}$$

Since $\mathscr{L}$ is self-adjoint, the φ_i can have the usual properties of orthonormality

$$\iiint \mathrm{d}\boldsymbol{x}\, \varphi_i(\boldsymbol{x})\varphi_j(\boldsymbol{x}) = \delta_{ij} \tag{5.45}$$

and completeness

$$\sum_i \varphi_i(\boldsymbol{x})\varphi_i(\boldsymbol{x}_0) = \delta(\boldsymbol{x} - \boldsymbol{x}_0) \,. \tag{5.46}$$

Motion in the phase space spanned by the a_i is nondivergent. The quadratic integral invariants are the energy

$$E = \sum_i \lambda_i^2 a_i^2 \tag{5.47}$$

and the enstrophy at level z

$$\Omega(z) = \sum_i \sum_j (\lambda_i^2 \lambda_j^2 a_i a_j - 2\lambda_i^2 a_i f_j) \iint \mathrm{d}x\, \mathrm{d}y\, \varphi_i(\boldsymbol{x})\, \varphi_j(\boldsymbol{x}) + \text{constants}\,. \tag{5.48}$$

The equilibrium probability distribution is

$$\hat{P} \propto \exp\left[-\alpha E - \int \gamma(z)\, \Omega(z)\, \mathrm{d}z\right], \tag{5.49}$$

where α and $\gamma(z)$ are Lagrange multipliers chosen such that $\langle E \rangle$ and $\langle \Omega(z) \rangle$ match their initial values. Since (5.49) is multivariate Gaussian, the equilibrium flow statistics are completely specified by the first and second moments $\langle a_i \rangle$ and $\langle a_i a_j \rangle$, or by the equivalent physical-space moments $\langle \psi(\boldsymbol{x}) \rangle$ and $\langle \psi(\boldsymbol{x}) \psi(\boldsymbol{x}_0) \rangle$. It is possible to get differential equations governing the latter directly from manipulations on (5.49). To derive these equations, note that (5.49) may be written in a standard form

$$P \propto \exp\left[-\tfrac{1}{2} \sum_i \sum_j A_{ij}\, a_i' a_j'\right], \tag{5.50}$$

where

$$A_{ij} = 2\alpha\lambda_i^2 \delta_{ij} + 2\lambda_i^2 \lambda_j^2 B_{ij}\,, \tag{5.51}$$

$$B_{ij} = \iiint \gamma(z)\, \varphi_i(\boldsymbol{x})\, \varphi_j(\boldsymbol{x})\, \mathrm{d}\boldsymbol{x} \tag{5.52}$$

and

$$a_i' \equiv a_i - \langle a_i \rangle\,. \tag{5.53}$$

Then

$$\langle a_i \rangle = 2 \sum_j \sum_l A_{ij}^{-1} \lambda_j^2 B_{jl} f_l \tag{5.54}$$

and

$$\langle a_i' a_j' \rangle = A_{ij}^{-1}, \tag{5.55}$$

where A^{-1} is the inverse of the matrix A. Now (5.55) implies that

$$\sum_i \sum_j \left[\sum_l A_{il} \langle a_i' a_j' \rangle\, \varphi_i(\boldsymbol{x})\, \varphi_j(\boldsymbol{x}_0)\right] = \sum_i \varphi_i(\boldsymbol{x})\, \varphi_i(\boldsymbol{x}_0) = \delta(\boldsymbol{x} - \boldsymbol{x}_0) \tag{5.56}$$

by (5.46). Substitution of (5.51) into the left-hand side of (5.56) and straightforward manipulations using (5.41)-(5.52) reduce (5.56) to

$$2\mathscr{L}[\gamma \mathscr{L} - \alpha] R(\boldsymbol{x}, \boldsymbol{x}_0) = \delta(\boldsymbol{x} - \boldsymbol{x}_0)\,, \tag{5.57}$$

where

$$R(\boldsymbol{x}, \boldsymbol{x}_0) = \langle \psi'(\boldsymbol{x})\, \psi'(\boldsymbol{x}_0) \rangle \tag{5.58}$$

and $\mathscr{L}'$ operates on $\boldsymbol{x}$. Similarly, the transform of (5.54) is

$$(\gamma \mathscr{L} - \alpha) \langle \psi \rangle + \gamma f = 0 \,, \tag{5.59}$$

which is analogous to (5.28). Equations (5.57), (5.59) completely determine the equilibrium state. For example, the equilibrium transient kinetic energy at $\boldsymbol{x}$ is

$$[\nabla \cdot \nabla_0 R(\boldsymbol{x}, \boldsymbol{x}_0)]_{\boldsymbol{x}_0 = \boldsymbol{x}} \,, \tag{5.60}$$

where

$$\nabla = \left(\frac{\partial}{\partial x}, \frac{\partial}{\partial y} \right) \quad \text{and} \quad \nabla_0 = \left(\frac{\partial}{\partial x_0}, \frac{\partial}{\partial y_0} \right). \tag{5.61}$$

The development leading up to (5.57), (5.59) can also be carried out directly in physical space, without reference to the eigenmodes of $\mathscr{L}$. Then, instead of the infinite-dimensional integrations, one has to deal with functional derivatives. Here the eigenmodes are purely a device for avoiding functional methods. An alternate device (which is less efficient in this case) would be to write the averages as functional integrals over physical space, replace derivatives by finite differences, perform the integrations required to get the moments of $\psi(\boldsymbol{x})$ and then pass back from differences to differentials. The same equations result.

Qualitative properties of the equilibrium state are obvious from (5.57). The operator $\mathscr{L}$ has the form of a diffusion operator with vertical-diffusion coefficient $f^2/\mathscr{N}^2$. Thus $R(\boldsymbol{x}, \boldsymbol{x}_0)$ corresponds to the equilibrium «temperature» distribution with a delta-function source at $\boldsymbol{x}_0$. The vertical boundaries are nonconducting. (The analogy is inexact because the diffusion operator acts twice. Also $\gamma(z)$ has general z-dependence.) We anticipate maximum transient energy in regions of strong stratification and small Coriolis parameter.

To investigate the funneling effect in its simplest form, consider N-layer quasi-geostrophic flow in an equatorial ($f = \beta y$) channel between walls at $y = \pm \pi L/2$. Let the layer depths and density jumps all be equal. Nondimensionalize the horizontal distance by L, time by L/U (where U is a characteristic velocity), vertical distance by the fluid depth D, and the streamfunction by UL. The nondimensional dynamics are

$$\frac{\partial q_i}{\partial t} + J(\psi_i, q_i) + \beta^* \frac{\partial \psi_i}{\partial x} = 0 \,, \tag{5.62}$$

where

$$q_i = \mathscr{L}_i[\psi_j] , \tag{5.63}$$

$$\mathscr{L}_i[\psi_j] = \nabla^2\psi_i + F_0 y^2 \sum_j T_{ij}\psi_j , \tag{5.64}$$

$$F_0 = N\beta^2 L^4/g' D , \qquad \beta^* = \beta L^2/U ,$$

and

$$[T_{ij}] = \begin{bmatrix} -1 & +1 & & & & \\ 1 & -2 & 1 & & & 0 \\ & 1 & -2 & 1 & & \\ & & \cdots & \cdots & \cdots & \\ & 0 & & 1 & -2 & 1 \\ & & & & +1 & -1 \end{bmatrix} .$$

Let the boundary conditions be

$$\psi(x, y) = \psi(x + 2\pi, y) \tag{5.65}$$

and

$$\psi\left(x, \pm\frac{\pi}{2} + y\right) = -\psi\left(x, \pm\frac{\pi}{2} - y\right) . \tag{5.66}$$

The analog of (5.57) is

$$2\mathscr{L}_i[\gamma_j \mathscr{L}_j[R_{mn}(\boldsymbol{x}, \boldsymbol{x}_0)] - \alpha R_{jn}(\boldsymbol{x}, \boldsymbol{x}_0)] = \delta(\boldsymbol{x} - \boldsymbol{x}_0)\,\delta_{in} . \tag{5.67}$$

Suppose γ_j is independent of $\hat{\jmath}$ (corresponding to an approximately uniform vertical initial energy distribution). It is then convenient to introduce the vertical-mode variables $\hat{\psi}_s$ defined by

$$\psi_i = \sum_{s=0}^{N-1} \hat{\psi}_s(x, y)\,\varphi_s(i) , \tag{5.68}$$

where

$$\varphi_s(i) = \sqrt{\frac{2 - \delta_{s0}}{N}} \cos\left[\left(i - \frac{1}{2}\right)\frac{s\pi}{N}\right] , \qquad i = 1, \ldots, N ,\ s = 0, \ldots, N-1 . \tag{5.69}$$

We find that

$$\langle\hat{\psi}_s(x, y)\,\hat{\psi}_{s_0}(x_0, y_0)\rangle = \hat{R}_s(x, y; x_0, y_0)\,\delta_{ss_0} \tag{5.70}$$

obeys

$$\hat{\mathscr{L}}_s(\hat{\mathscr{L}}_s - \alpha/\gamma)\,\hat{R}_s = \frac{1}{2\gamma}\,\delta(x - x_0)\,\delta(y - y_0) , \tag{5.71}$$

where

$$\hat{\mathscr{L}}_s \equiv \nabla^2 - \varepsilon_s^{-2} y^2 \tag{5.72}$$

and

$$\varepsilon_s = \left[2\sqrt{F_0} \sin \frac{s\pi}{2N} \right]^{-1} \tag{5.73}$$

is the (nondimensional) s-th deformation radius. In this geometry $\sum_i \overline{q_i^2}$ and $\sum_i \overline{q_i y}$ are separately conserved. If the latter is zero initially, then there is no equilibrium mean flow, and the enstrophy invariant reduces to

$$\Omega = \sum_i \overline{\mathscr{L}_i [\psi_i]^2} = \sum_s \overline{\hat{\mathscr{L}}_s (\hat{\psi}_s)^2} \equiv \sum_s \hat{\Omega}_s \,. \tag{5.74}$$

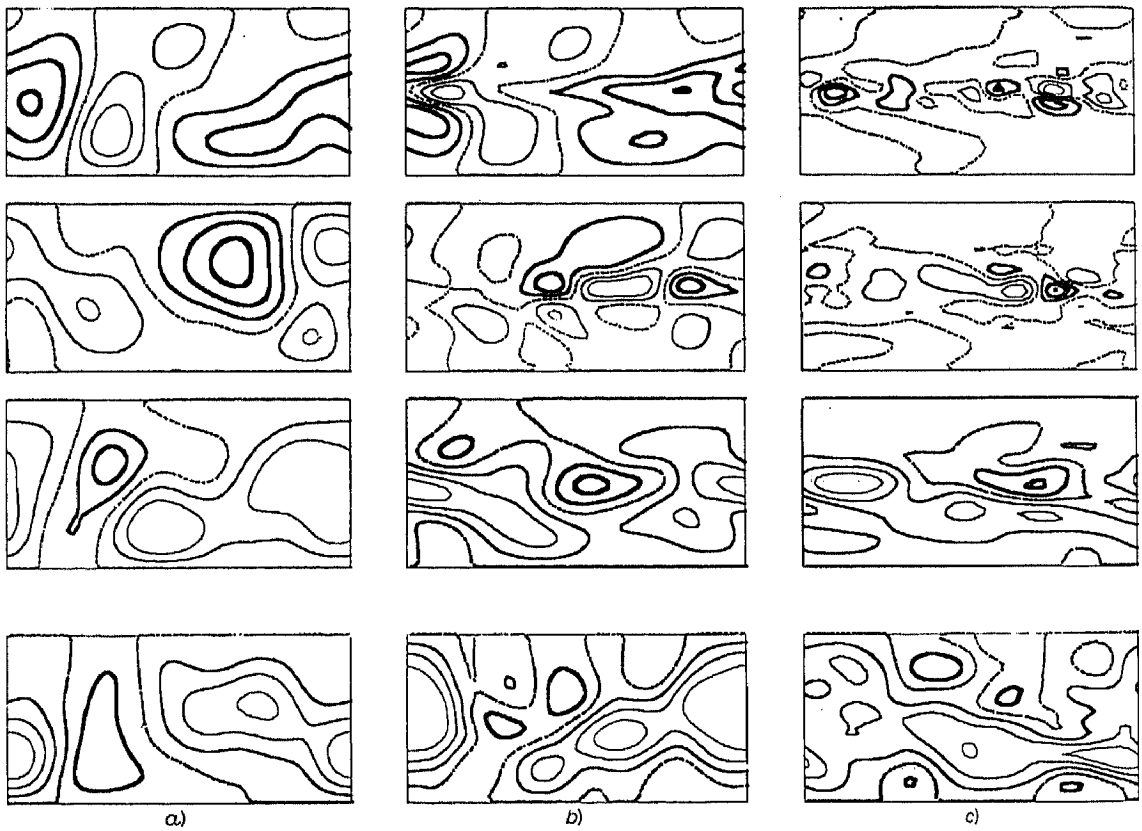

Fig. 7. – The vertical-mode streamfunctions $\hat{\psi}_s$ in the equatorial channel ($0 < x < 2\pi$, $-\pi/2 < y < \pi/2$) for the barotropic mode $s = 0$ (bottom), $s = 1$, $s = 3$ and $s = 5$ (top). The equator lies along the axis of the channel. *a*) weeks = 0, *b*) weeks = 3.346, *c*) weeks = 23.421.

Fig. 8. – The kinetic energy averaged over x in the vertical modes $s = 0, 1, 2, 3, 4, 5$. The equator lies at $y = 0$. *a*) weeks = 0, *b*) weeks = 10, *c*) weeks = 30.

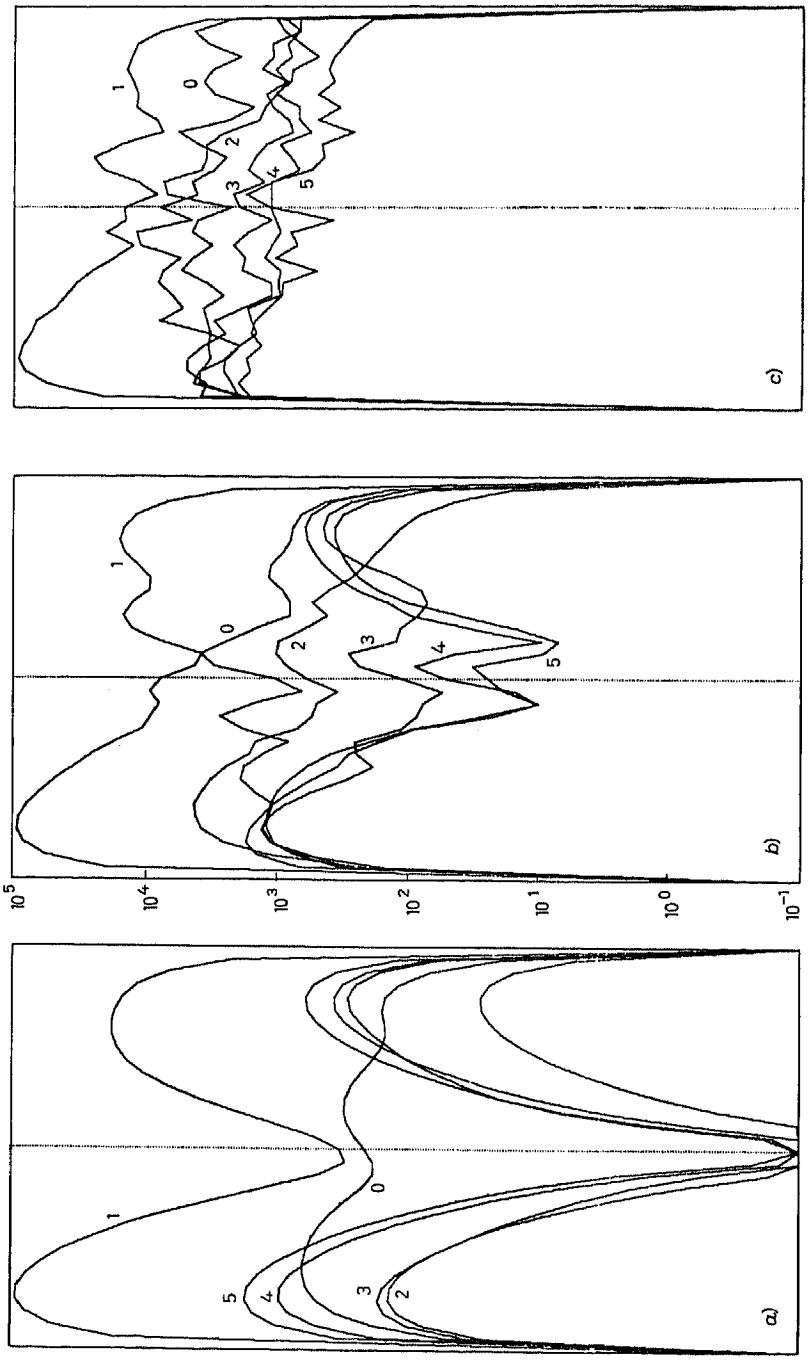

Fig. 9. – The quantity Ω_s in vertical modes $s = 0, 1, 2, 3, 4, 5$. *a*) weeks = 0, *b*) weeks = 10, *c*) weeks = 30.

For the barotropic mode ($s = 0$), the equilibrium energy is independent of latitude and maximum at wave number α/γ. For the baroclinic modes ($s \neq 0$), $\varepsilon_s^2 \alpha/\gamma$ is small and

$$(\nabla^2 - \varepsilon_s^{-2} y^2)^2 \hat{R}_s = \frac{1}{2\gamma} \delta(\boldsymbol{x} - \boldsymbol{x}_0) \tag{5.75}$$

has solutions of the form

$$\hat{R}_s = \frac{\varepsilon_s}{2\gamma} \Phi\left(\frac{\boldsymbol{x}}{\varepsilon_s^{\frac{1}{2}}}, \frac{\boldsymbol{x}_0}{\varepsilon_s^{\frac{1}{2}}}\right), \tag{5.76}$$

where

$$(\nabla^2 - y^2)^2 \Phi(\boldsymbol{x}, \boldsymbol{x}_0) = \delta(\boldsymbol{x} - \boldsymbol{x}_0) \tag{5.77}$$

(independent of ε_s). Thus the equatorial peak in the kinetic energy in vertical mode s has latitudinal width $\varepsilon_s^{\frac{1}{2}}$, or dimensionally

$$\left(\frac{g' H}{\beta^2}\right)^{\frac{1}{4}} \sin^{-\frac{1}{2}} \frac{s\pi}{2N}, \tag{5.78}$$

where H is the layer thickness. This region narrows with increasing s, but (5.60) and (5.76) imply that the equilibrium kinetic energy at $y = 0$ is independent of s in this case. Thus equatorial confinement is sharpest for the higher vertical modes. For $|y| \gg \varepsilon_s^{\frac{1}{2}}$ (5.75) is solved approximately by treating y^2 as a constant on the left-hand side. To the same order of approximation $\hat{\Omega}_s$ is independent of latitude.

Figures 7-9 show the evolution of a six-layer inviscid quasi-geostrophic ocean in the equatorial beta-plane channel. The initial streamfunction is random and the kinetic energy is invariant with depth and equally divided between the barotropic and first baroclinic modes. The channel is 6000 by 3000 km and the energy density is $1.2 \cdot 10^8$ erg·cm. After only 23 weeks, high vertical-mode kinetic energy is strongly trapped at the equator and $\hat{\Omega}_s$ is nearly independent of latitude.

6. – Closure.

Real turbulence is often far from the state of absolute equilibrium considered in the previous section. Unfortunately, no fully satisfactory nonequilibrium theory exists. Straightforward averaging of the equations of motion yields an unclosed hierarchy of statistical moment equations in which the evolution equation for the n-th moment always contains the $(n+1)$-th moment. This is the « closure problem ». All known methods for closing the moment equations involve additional physical assumptions not deducible from the equations of motion.

This section discusses relatively simple second-moment single-time closures which are representative of the closures used in application-oriented studies. These closures (and others of the « direct interaction » group) can be « derived » by a variety of perturbationlike procedures, none of which pretends to mathematical rigor. The derivations lead to moment equations which always resemble Boltzmann's collision equation for a gas of hard spheres. This structure is virtually guaranteed, if the moment equations are to satisfy certain consistency properties. However, the best justification for these closures is the usually good agreement between their predictions and direct computer simulations of the equations of motion [24].

A traditional goal of closure theory is to extend the spatial resolution (or Reynolds number) beyond that attainable in direct numerical simulations of the equations of motion. However, quasi-geostrophic dynamics obtain over less than three wave number octaves in the ocean and two in the atmosphere. This resolution is within the reach of modern computers. Still, closure is a useful tool for interpreting the statistics obtained by averaging the direct simulations. For example, closure theory can compute the effects of one statistic on another in a way that permits analytical simplifications after the dominant terms are identified. Unfortunately, the complexity of the theory can increase prohibitively if statistical symmetries (such as spatial homogeneity) are relaxed.

Let the equations of motion again be

$$\dot{y}_i = \sum_{j,l} A_{ijl} y_j y_l - v_i y_i \,, \tag{6.1}$$

where

$$A_{ijl} = A_{ilj} \,, \tag{6.2}$$

with no loss in generality. The coupling coefficients also satisfy the Liouville property

$$A_{iij} = 0 = A_{iji} \,. \tag{6.3}$$

For simplicity we assume

$$\langle y_i \rangle = 0 \qquad \text{and} \qquad \langle y_i(t)\, y_j(t) \rangle = Y_i(t)\, \delta_{ij} \,, \tag{6.4}$$

which are equivalent to horizontal statistical homogeneity.

The eddy-damped Markovian (EDM) model [25, 26] closes the moment hierarchy by discarding fourth cumulants. A « cumulant » is the difference between a moment and the value it would have if all the variables were Gaussian. Direct averaging of (6.1) yields

$$\left(\frac{\mathrm{d}}{\mathrm{d}t} + 2v_i\right) Y_i = 2 \sum_{j,l} A_{ijl} \langle y_i y_j y_l \rangle \tag{6.5}$$

and

$$(6.6)\qquad \left(\frac{\mathrm{d}}{\mathrm{d}t}+v_i+v_j+v_l\right)\langle y_i y_j y_l\rangle = \sum_{m,n}\{A_{imn}\langle y_m y_n y_j y_l\rangle + A_{jmn}\langle y_m y_n y_i y_l\rangle + A_{lmn}\langle y_m y_n y_j y_i\rangle\}\,.$$

If A, B, C, D are Gaussian variables, then

$$(6.7)\qquad \langle ABCD\rangle = \langle AB\rangle\langle CD\rangle + \langle AC\rangle\langle BD\rangle + \langle AD\rangle\langle BC\rangle\,.$$

Apply this factorization to the right-hand side of (6.6), solve (6.6) for $\langle y_i y_j y_l\rangle$, and substitute the result into (6.5). Then (6.5) becomes

$$(6.8)\qquad \left(\frac{\mathrm{d}}{\mathrm{d}t}+2v_i\right)Y_i = \sum_{j,l}\int_0^t \mathrm{d}s\,\exp[-(t-s)(v_i+v_j+v_l)]\cdot \cdot\{4(A_{ijl})^2 Y_j(s)\,Y_l(s) + 8A_{ijl}A_{jil}\,Y_l(s)\,Y_i(s)\}\,.$$

Unfortunately, numerical solutions of (6.8) lead to unphysical large negative energy ($Y_i < 0$) when the Reynolds number is large. To see why, identify subscript i with wave number $\boldsymbol{k}$, and imagine that the initial spectrum has a sharp peak (fig. 10). Soon after $t = 0$, the right-hand side of (6.8) is large and negative for wave numbers inside the peak and large and positive for those outside. At even later times, the magnitude of the term in curly brackets in (6.8) decreases, but the fluid still remembers the initial large tendencies, because the time integration in (6.8) runs all the way back to $t = 0$. The limit of large Reynolds number corresponds to $v_i, v_j, v_l \to 0$ in (6.8), and in this limit the values of the term in curly brackets in the distant past ($s \ll t$) are weighted equally with those of the near past ($s \approx t$). Consequently the large initial tendencies are never forgotten and the plunging spectral peak shoots right through the zero level. The cause of this « sling shot » effect is easily seen to be the inefficiency of memory cut-off in the model as the $v_i \to 0$.

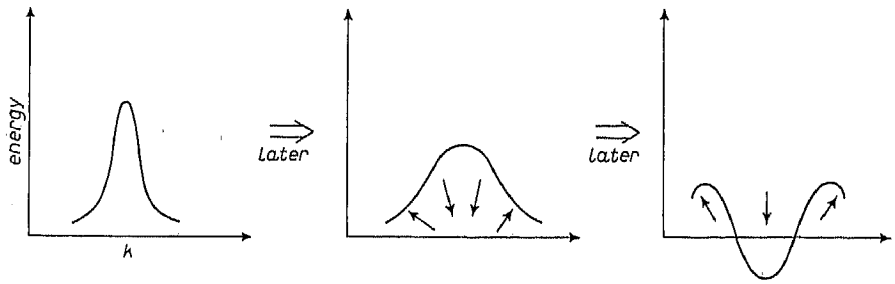

Fig. 10. – Failure of quasi-normal closure (6.8).

In real turbulence, past states are forgotten not because of the viscosity but as a result of nonlinear scrambling of the fluid by itself. At large Reynolds numbers the memory time should become independent of the viscosity, in contradiction with (6.8). These remarks suggest that (6.8) can be repaired by replacing v_i, v_j, v_l, on the right-hand side only, with augmented viscosities μ_i, μ_j, μ_l which measure the scrambling effect of the flow on itself. The μ_i differ from the familiar « eddy viscosity » of fluid mechanics in that they enter (6.6) but not (6.5) and, therefore, do not directly augment the dissipation of energy. Since the μ_i ought to be increasing functions of the Reynolds number, at large Reynolds number it might become accurate to replace the term in curly brackets of (6.8) (with the μ_i inserted) with its value at $s = t$. The latter (Markovization) step eliminates nonsimultaneous covariances. The result is

$$\left(\frac{\mathrm{d}}{\mathrm{d}t} + 2v_i + 2n_i\right) Y_i = \sum_{j,l} \theta_{ijl}\{4(A_{ijl})^2 Y_j Y_l\} , \tag{6.9}$$

where

$$n_i = -4 \sum_{j,l} \theta_{ijl} A_{ijl} A_{jil} Y_l , \tag{6.10}$$

$$\frac{\mathrm{d}}{\mathrm{d}t}\theta_{ijl} = 1 - (\mu_i + \mu_j + \mu_l)\theta_{ijl} \tag{6.11}$$

and

$$\theta_{ijl}(0) = 0 , \tag{6.12}$$

corresponding to precisely Gaussian initial conditions.

Equations (6.9)-(6.12) comprise the EDM. It is easy to show that the EDM does not allow $Y_i < 0$. Note that

$$\theta_{ijl} \to \frac{1}{\mu_i + \mu_j + \mu_l} \qquad \text{as } t \to \infty . \tag{6.13}$$

The parameters μ_i can be prescribed heuristically. For example,

$$\mu_k^2 = \int_0^k k^2 \mathscr{E}(k, t)\, \mathrm{d}k \tag{6.14}$$

equates the memory time to the time required for larger-scale flow to strain an eddy of size k^{-1}.

The EDM has several desirable consistency properties. First, it automatically conserves any quadratic invariant which is conserved by the exact dynamics. Second, it predicts only realizable statistics. (Negative energies can never appear.) Third, EDM is consistent with the second law. This third property

requires elaboration. From the point of view of EDM, the $Y_i(0)$ are given initially and the closure predicts $Y_i(t)$ at all future times. However, the initial conditions correspond to many possible exact specifications of the y_i which together fill a finite volume in phase space like that of fig. 4. Since the averages predicted by EDM are phenomenological (no pretense is made of actually solving the equations of motion), EDM must be consistent with the principle of continuous increase in entropy. To calculate the entropy at time t corresponding to a knowledge of all the $Y_i(t)$, maximize S subject to the normalization requirement and

$$\langle y_i^2 \rangle = Y_i \,, \qquad \text{all } i \,. \tag{6.15}$$

The result is

$$P = \exp\Big[\lambda - \sum_i \alpha_i y_i^2\Big] \,, \tag{6.16}$$

where

$$\lambda = \tfrac{1}{2} \sum_i \ln(\alpha_i/\pi) \tag{6.17}$$

and

$$\alpha_i = 1/2\, Y_i \,. \tag{6.18}$$

The entropy is thus

$$S = -\frac{1}{2} \sum_i \Big[\ln\Big(\frac{\alpha_i}{\pi}\Big) + \frac{1}{2}\Big] \,, \tag{6.19}$$

and we must, therefore, require

$$\frac{\mathrm{d}}{\mathrm{d}t} \sum_i \ln Y_i \geqslant 0 \,, \tag{6.20}$$

where the tendencies are those resulting from the nonlinear terms in the closure. Note that absolute equilibrium may be deduced directly by maximizing the sum in (6.20) subject to total-energy and enstrophy conservation.

To see that EDM satisfies these consistency properties, note that (6.9), (6.10) can also be obtained by the following formal procedure. Let $v_i = 0$ and expand the exact dynamics in a Taylor series about $t = 0$:

$$y_i(t) = y_i(0) + t \sum_{j,l} A_{ijl} y_j(0) y_l(0) + t^2 \sum_{j,l} \sum_{m,n} A_{ijl} A_{lmn} y_j(0) y_m(0) y_n(0) + \cdots \,. \tag{6.21}$$

Let the $y_i(0)$ be Gaussian. Then squaring and averaging (6.21) gives

$$Y_i(t) = Y_i(0) + 2t^2 \sum_{j,l} (A_{ijl})^2 Y_j(0) Y_l(0) + \\ + 4t^2 \sum_{j,l} A_{ijl} A_{jil} Y_l(0) Y_i(0) + O(t^4) \,. \tag{6.22}$$

Truncate (6.22) after $O(t^2)$, differentiate with respect to time, and then restore all arguments to t. After these alterations (6.22) reads

$$\dot{Y}_i(t) = \sum_{j,l} t\{\tfrac{1}{4}(A_{ijl})^2\, Y_j(t)\, Y_l(t) + 8A_{ijl}A_{jil}\, Y_l(t)\, Y_i(t)\}\,, \tag{6.23}$$

which becomes identical with (6.9), (6.10) if the factor t is replaced by the triad decorrelation time θ_{ijl}. The conservation and realizability properties hold for (6.23), because the same properties hold term by term for the Taylor series expansion of the exact dynamics. The generalization to (6.9), (6.10) is easy. (Sum the contributions of individual triads.) The inequality (6.20) can be verified directly, but also as follows. The difference between the entropy at time t and time zero is

$$S(t) - S(0) = -\int[\hat{P}(t)\ln\hat{P}(t) - \hat{P}(0)\ln\hat{P}(0)] \tag{6.24}$$

(by definition),

$$= -\int[\hat{P}(t)\ln\hat{P}(t) - P(0)\ln P(0)] \tag{6.25}$$

(because the initial distribution is Gaussian by assumption),

$$= -\int[\hat{P}(t)\ln\hat{P}(t) - P(t)\ln P(t)] \tag{6.26}$$

(by (5.9)). Thus

$$S(t) - S(0) \geqslant 0\,, \tag{6.27}$$

because $\hat{P}(t)$ is, by definition, the distribution that maximizes $S(t)$. As $t \to 0$, (6.23) becomes exact. Therefore, (6.23) must be consistent with $\mathrm{d}S(t)/\mathrm{d}t > 0$.

It is useful to realize that the EDM closure is exact for the model equation

$$\left(\frac{\mathrm{d}}{\mathrm{d}t} + 2n_i\right) y_i = W(t) \sum_{j,l} (\theta_{ijl})^{\frac{1}{2}} y_j^{\mathrm{G}} y_l^{\mathrm{G}}\,, \tag{6.28}$$

where n_i is given by (6.10), $W(t)$ is a white-noise process with

$$\langle W(t)\, W(t')\rangle = 2\delta(t - t')\,, \tag{6.29}$$

and y_i^{G} is a Gaussian field with the same covariance as y_i. Conversely, if (6.28) is proposed *a priori* as a stochastic model for (6.1), then the only choice for the nonrandom damping coefficient n_i that satisfies the consistency properties is that given by (6.10).

The derivation of (6.23) by expansion in time is very similar to Hasselmann's original derivation of his weak wave equations. The difference is,

loosely speaking, that the leftover factor of t in (6.23) is « used up » by the requirement that the interactions be resonant. In fact, waves incorporate easily into EDM [27]. Suppose, for example, that (6.1) is generalized to

$$\dot{y}_i + \sqrt{-1}\,\omega_i = \sum_{j,l} A_{ijl} y_j y_l\,, \qquad \omega_i = \text{const}\,. \tag{6.30}$$

If the steps leading to (6.9)-(6.12) are repeated, (6.9), (6.10) are unchanged, but (6.13) becomes

$$\theta_{ijl} \to \frac{\mu_i + \mu_j + \mu_l}{(\mu_i + \mu_j + \mu_l)^2 + (\omega_i + \omega_j + \omega_l)^2} \qquad \text{as } t \to \infty\,. \tag{6.31}$$

If weak turbulence corresponds to the limit $\mu \to 0$, then

$$\theta_{ijl} \to \pi\delta(\omega_i + \omega_j + \omega_l) \tag{6.32}$$

and EDM reduces to the weak wave equations (assuming the possibility of tertiary resonant interactions). However, it may be unrealistic to eliminate off-resonant interactions completely. For example, particular dispersion relations might allow no pathway to absolute equilibrium.

The above closures can be viewed as abridgments of Kraichnan's [28] direct interaction approximation (DIA). The independent variables in the DIA are the nonsimultaneous covariances $\langle y_i(t)\, y_i(t')\rangle$ and an averaged Green's function which measures the response of each mode to an infinitesimal excitation in the presence of all the other modes. Loosely speaking, this response function replaces the decorrelation time factors θ_{ijl} above. The DIA is entirely self-contained; there are no unspecified parameters or undetermined constants. Unfortunately, however, the DIA demands integrations back over the lag times and these greatly increase computing requirements. Additionally, the decorrelation time implied by the DIA response functions confuses the memory time scale for true flow distortion with the advective time scale for sweeping of small structures past a fixed point by larger eddies in the flow. This defect is sometimes described by the statement that « the DIA is not invariant with respect to random Galilean transformations ». Because of Galilean noninvariance, the DIA erroneously predicts a $k^{-3/2}$ inertial-range power law instead of the $k^{-5/3}$ Kolmogorov range.

The Markovian closures require many fewer computations and storages than DIA and the freedom to specify the decorrelation times μ_i^{-1} offers a way to ensure Galilean invariance. The test field model [29] separates the effects of random displacements from true distortion by relating the decorrelation time to the time required for an initially incompressible flow to develop a compressible component if pressure forces (and the constraint to conserve mass) are suddenly switched off. For a sufficiently steep spectrum the test field

prescription reduces to (6.14). Unfortunately, the test field model has no clear generalization to more complicated dynamics. However, many results are rather insensitive to the precise form of θ_{ijl}.

Closure applications relevant to geostrophic turbulence include studies of the two-dimensional inertial ranges [30], eddy viscosity [31], predictability [32, 33], the decay of anisotropy [34], two-dimensional turbulence on the beta-plane [20, 27] and over random topography [35, 36], decaying stratified quasi-geostrophic turbulence [37] and forced two-layer turbulence [10, 38]. The next section considers beta-plane turbulence in some detail.

7. – Beta-plane turbulence.

Consider two-dimensional turbulence on the beta-plane, governed by

$$\frac{\partial \varrho}{\partial t} + J(\psi, \varrho) + \beta \frac{\partial \psi}{\partial x} = \nu \nabla^2 \varrho \,, \tag{7.1}$$

where

$$\varrho = \nabla^2 \psi \,. \tag{7.2}$$

These equations differ from (3.1) only in the presence of the linear beta term, which gives rise to Rossby waves. The Rossby-wave properties of dispersion and anisotropy make beta-plane turbulence an ideal testing ground for general ideas about waves in turbulence. Let the flow be infinitely periodic, that is

$$\psi(x, y) = \psi(x + L_p, y) = \psi(x, y + L_p) \tag{7.3}$$

for all x and y and some L_p. Then the integral invariants (energy and enstrophy) and absolute-equilibrium states are the same as for two-dimensional turbulence, and are independent of beta. The nonequilibrium flow is, however, drastically affected by the Rossby waves. At the scales of motion at which the wave steepness (the ratio of particle to phase speeds) falls below unity, wave dispersion inhibits nonlinear interactions and the flow favors zonal (east-west) currents. The supposedly isotropic final state is thus approached via phase-space pathways which exhibit considerable anisotropy.

The Fourier transform of (7.1) is

$$\left(\frac{\mathrm{d}}{\mathrm{d}t} + i\omega_k\right) \psi_k + \sum_{p+q=k} (p_x q_y - q_x p_y)\, q^2/k^2 \psi_p \psi_q = 0 \,, \tag{7.4}$$

where

$$\omega_k = -\beta k_x / k^2 . \tag{7.5}$$

In the small-amplitude limit, solutions to (7.4) are superposed Rossby waves with the dispersion relation (7.5). These waves all have westward phase velocities and wave periods which decrease as the wavelength increases (for fixed direction of propagation). For fixed frequency, nondimensionalize $\boldsymbol{k}$ by β/ω. Then (7.5) is a circle on the (k_x, k_y)-plane with center at $(-\frac{1}{2}, 0)$ and unit diameter. The group velocity is

$$\left(\frac{\partial\omega}{\partial k_x}, \frac{\partial\omega}{\partial k_y}\right) = \frac{\omega^3}{\beta}\left(\frac{2k^2-1}{k^2}, \pm\frac{\sqrt{1-k^2}}{k}\right). \tag{7.6}$$

Thus long waves ($k < 2^{-1/2}$) carry energy westward at a speed that approaches $\omega^3/\beta k^2$ as $k \to 0$. Short waves move energy eastward at a much slower speed. The region affected by an initially concentrated disturbance, therefore, lies principally to the west. This property explains why intense boundary currents like the Gulf Stream are found at western boundaries.

For motions of length scale L and characteristic velocity U, the size ratio of the beta term to the nonlinear terms in (7.1) is $\beta L^2/U$. RHINES [9, 22] proposed that the wave number $k_\beta \equiv \sqrt{\beta/U}$ typically separates a « wave regime » at $k < k_\beta$ from a « turbulence regime » at $k > k_\beta$. In the ocean, $k_\beta^{-1} \approx 70$ km. Suppose that the energy is initially concentrated at wave number $k_1 \gg k_\beta$. By the reasoning of sect. **3**, which holds whether beta is present or not, the energy moves steadily into lower wave numbers. When the energy reaches k_β, however, Rossby waves begin to propagate freely, as the wave period becomes shorter than an eddy turn-over time. The transition is abrupt because the Rossby-wave dispersion relation (7.5) and the « dispersion relation » for the turbulence, $\omega = Uk$, have opposite slopes. The analog of (6.8) for (7.4) is

$$\begin{aligned}\frac{\mathrm{d}}{\mathrm{d}t}U_{\boldsymbol{k}} = \sum_{\boldsymbol{p}+\boldsymbol{q}=\boldsymbol{k}} \frac{|\boldsymbol{k}\times\boldsymbol{p}|^2}{k^2p^2q^2}\int_0^t \mathrm{d}s\, \exp\left[-(\mu_q+\mu_p+\mu_k)(t-s)\right]\cdot \\ \cdot\cos\left[(\omega_q+\omega_p+\omega_{-k})(t-s)\right]\cdot \\ \cdot\left\{(p^2-q^2)^2\, U_p(s)\, U_q(s) - 2(q^2-p^2)(k^2-p^2)\, U_k(s)\, U_p(s)\right\},\end{aligned} \tag{7.7}$$

where $U_{\boldsymbol{k}}$ is the energy in wave number $\boldsymbol{k}$ and μ_k^{-1} is the time for the turbulence to deform an eddy of size k^{-1}. In the wave regime, $\omega \gg \mu$ and the oscillating factor in (7.7) greatly reduces energy transfer unless

$$\omega_p + \omega_q = \omega_k\,, \tag{7.8}$$

which is the condition for resonance. We thus expect energy transfer to lower wave numbers to proceed much more slowly in the wave regime. Nondispersive waves would satisfy (7.8) automatically.

Markovization of (7.7) gives the analog of (6.9), namely

$$\frac{\mathrm{d}}{\mathrm{d}t} U_k = \sum_{p+q=k} \frac{|\boldsymbol{k}\times\boldsymbol{p}|}{k^2 p^2 q^2} \theta_{kpq} \{\text{same as (7.7)}\}, \tag{7.9}$$

where

$$\theta_{kpq} = \frac{\mu_k + \mu_p + \mu_q}{(\mu_k + \mu_p + \mu_q)^2 + (\omega_p + \omega_q + \omega_{-k})^2}. \tag{7.10}$$

Again,

$$\theta_{kpq} \to \pi\delta(\omega_p + \omega_q + \omega_{-k}) \tag{7.11}$$

in the limit of weak turbulence ($\mu/\omega \to 0$). The resonance condition (7.8) can be viewed as a selection rule on frequencies analogous to

$$\boldsymbol{p} + \boldsymbol{q} = \boldsymbol{k} \tag{7.12}$$

for wave numbers. The two together are a formidable constraint on triads that can transfer energy [39]. However, perfect resonance is too stringent a requirement. Instead, (7.10) shows that, if (7.8) is satisfied to within $O(\mu)$, then the interaction is as good as resonant. In the turbulence regime ($\mu \gg \omega$) the efficiency of energy transfer decreases with increasing μ, but in the wave regime ($\mu \ll \omega$) the efficiency can increase with μ, because the turbulence allows energy transfer in slightly off-resonant triads.

The appearance of anisotropy at low wave numbers is also expected. Consider a triad of wave vectors satisfying (7.12) with $p \geqslant q \geqslant k$. We continue to be interested in the case in which average energy transfer is into the lowest wave number k. Let $\varepsilon = k/p$ be small. Then

$$\boldsymbol{q} = -\boldsymbol{p}(1 + O(\varepsilon)) \tag{7.13}$$

and

$$\omega_p + \omega_q + \omega_{-k} = -\frac{\beta}{k}\left(\frac{k_x}{k} + O(\varepsilon^2)\right). \tag{7.14}$$

The ω_p, ω_q terms are of minor importance for two reasons. First, they cancel in sign. Second, the wave frequency is inversely proportional to wave number. If k lies within the wave regime, then this reasoning suggest dominant transfer into wave vectors k with $k_x/k_y = O(\varepsilon^2)$. Weak wave theory predicts that only the highest-frequency component is unstable to infinitesimal perturbations in an isolated triad [40]. RHINES [22] thus notes that zonal anisotropy can also be anticipated as the necessary consequence of energy transfer to low wave numbers *and* low frequencies.

Numerical experimental [9, 20, 22, 27] confirm these qualitative predictions. Figure 11 shows the enstrophy spectra after six turn-over times in three independent experiments with zero ($k_\beta = 0$), moderate ($k_\beta \approx 2$) and strong beta ($k_\beta \approx 4$). The common initial condition is a narrow spectral peak at $k = 10$. Zonal anisotropy is apparent in both the streamfunction and vorticity

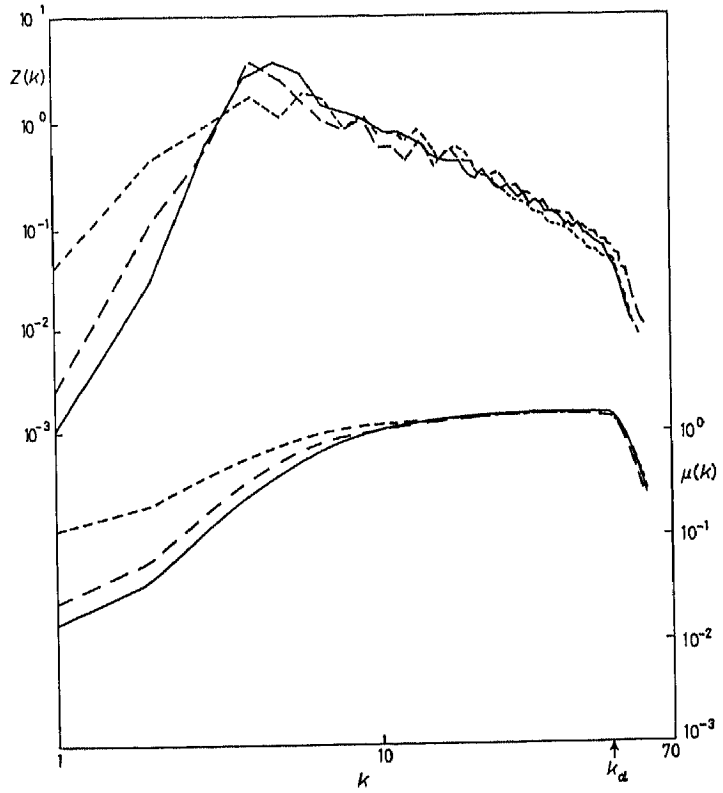

Fig. 11. – Enstrophy spectra after six turn-overs of beta-plane turbulence with zero (short dashes), moderate (= 12.5) (long dashes) and strong (= 25) (solid) beta. Courtesy of G. HOLLOWAY.

fields in the beta cases (fig. 12). HOLLOWAY [27] examines these experiments using the closure (7.9) with μ_k given by the test field model. He approximates the modal enstrophy spectrum $\langle \varrho_k \varrho_{-k} \rangle$ with the truncated angular expansion

$$2\pi k \langle \varrho_k \varrho_{-k} \rangle = Z(k)(1 - R(k) \cos 2\varphi_k) \,, \tag{7.15}$$

where φ_k is the angle between k and the k_x-axis. Positive $R(k)$ corresponds to zonal flow. Figure 13 shows $R(k)$ for the experiment with moderate beta along with closure estimates of $R(k)$ for three values of the adjustable para-

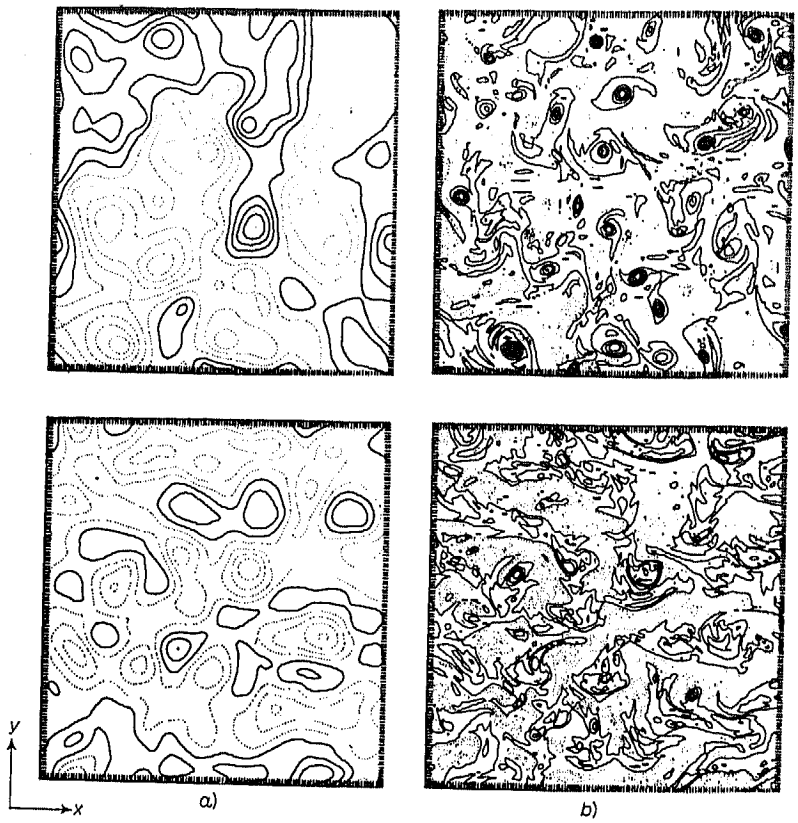

Fig. 12. – Streamfunction (a)) and vorticity (b)) fields after six turn-overs in the experiments with zero (top) and strong (=25) beta (bottom). Courtesy of G. HOLLOWAY.

meter in the test field model. As expected, zonal anisotropy is largest for $k < k_\beta$, but $R(k)$ has a secondary maximum at large k. Closure theory traces the high-wave-number anisotropy to the indirect effect of straining of the small-scale eddies by the large-scale zonal motion. The importance of this phenomenon is anticipated by Herring's [34] study of the decay of anisotropy in two-dimensional turbulence.

An isolated energetic patch within a broad quiescent region of fluid offers maximum contrast to the initially narrow spectral peak. Numerical experiments without beta confirm that both the patch diameter and dominant eddy size increase until the patch holds too few eddies to maintain turbulence [9]. Noting that the westward group velocity of large Rossby waves is proportional to the square of the wavelength, RHINES [22] conjectures that a turbulent patch on the beta-plane would, after an initial period of possibly slow growth, radiate energy quickly over a wide area. Turbulence would cease as particle speeds decrease within the growing patch. Approximately the maxim holds:

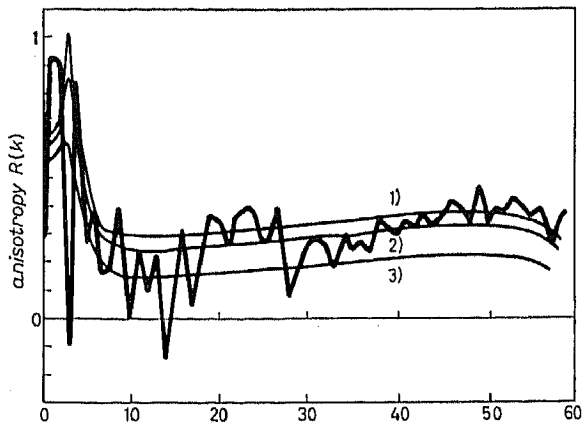

Fig. 13. – The simulated (heavy curve) and theoretical anisotropy spectrum $R(k)$ for beta-plane turbulence. The theoretical curves corresponds to three values of the adjustable parameter in the test field model: 1) $\lambda = 0.6$, 2) $\lambda = 0.7$, 3) $\lambda = 1.0$. Courtesy of G. HOLLOWAY.

Waves move energy rapidly through physical space, but inhibit energy transfer in wave number space. Turbulence the opposite.

The end state of beta-plane turbulence is controversial. (The question may be well be irrelevant to the relatively highly damped geophysical fluids, but not perhaps to the circulation on Jupiter [41].) The absolute-equilibrium state is a « best guess » by the criteria in sect. **5**, but it could be misleading if « mixing » in phase space ceases after the fluid enters the wave regime. RHINES [22] suggests steady zonal currents with alternating flow directions and length scale k_β^{-1} that would satisfy the linear-stability criterion

$$\beta - u_{yy} \neq 0 .$$

Rossby wave solitons are another, intriguing possibility.

8. – Comments.

Two themes pervade these lectures. The first is that weak, integral statements of fundamental conservation principles can anticipate distinctive flow characteristics. The idea succeeds because potential-enstrophy conservation is a strong constraint on quasi-geostrophic flow, and because higher-order invariants (ultimately, potential-vorticity conservation on particles) have apparently spotty projections on the phase-space manifolds corresponding to fixed values of the energy and enstrophy.

The second theme is the common tendency for natural systems to seek a

state of maximum disorder. This principle crept almost unnoticed into the discussion of sect. 3 in the suppositions that a narrow spectral peak would broaden, and that material lines and wave vectors lengthen on the average. It attained the status of a mathematical inequality (the second law) in sect. 5, and in sect. 6 combined with the weak-conservation principle to form the basis for closure.

The statistical-moment hierarchy was closed at the considerable price of replacing the ensemble of realizations of the exact dynamics by an ensemble of realizations of a stochastic model equation which conserves squared vorticity only in the spatial and ensemble average, but respects the idea of continuous mixing in phase space. The trade-off is between resemblance to the true dynamics and the possibility of getting simple closed equations for the statistics. Ironically, these closures seem better suited to address the relatively broad issues that arise in the rich quasi-geostrophic dynamics than more esoteric questions.

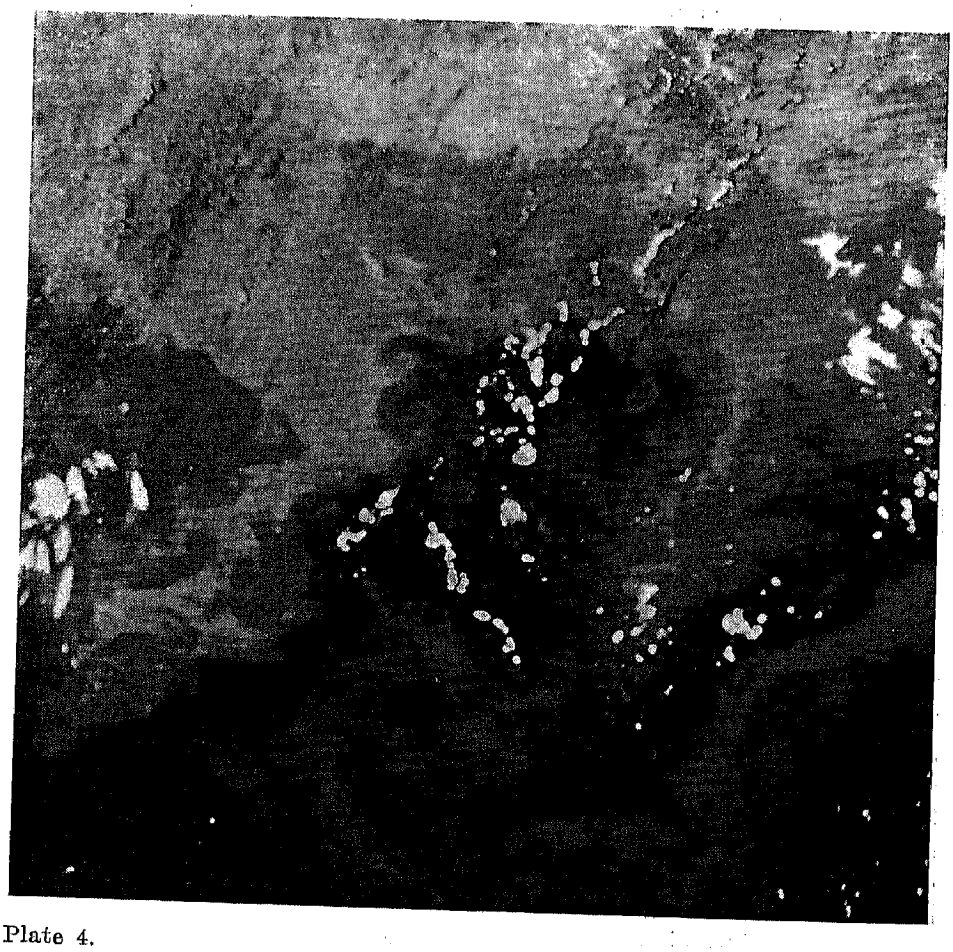

Plate 4.

about pure Navier-Stokes turbulence. However, applications to still more complicated, particularly inhomogeneous situations will require even further simplifications in the theory. The model viewpoint suggests a course: Retain the idea of a stochastic model, but relax even further the imposed requirements.

The broad goal of the theory is to deduce the major features of the observed circulation qualitatively but exclusively from first physical principles. Progress toward this end has been excruciatingly slow, consistently lagging the observations themselves. Modern observations show that the ocean is a perplexing mixture of order and apparent chaos. An infra-red photo of sea surface temperature offers a striking illustration (plate 4). The photo covers an area 560 km square centered on 29° N, 144° W in the Pacific. The maximum temperature contrast is about 1.5 °C. The photo was obtained by M. VAN WOERT of Scripps. It shows the subtropical front, a long semi-permanent boundary between cool (light-colored) northern water and warm (dark) water to the south. (The small white spots are clouds.) The explanation for the front may well lie within the realm of the linear quasi-laminar theories of basinscale wind-driven circulation, but the photo shows how the frontal boundary is broken up by turbulence. The large whorls have deformation scale.

* * *

I am funded by the National Science Foundation, IDOE (OCE 78-25670) as a part of Polymode.

REFERENCES

[1] J. PEDLOSKY: *Geophysical Fluid Dynamics* (New York, N. Y., 1979).
[2] L. ONSAGER: *Suppl. Nuovo Cimento*, **6**, 279 (1949).
[3] R. FJORTOFT: *Tellus*, **5**, 225 (1953).
[4] R. H. KRAICHNAN: *Phys. Fluids*, **10**, 1417 (1967).
[5] G. K. BATCHELOR: *Phys. Fluids*, **12**, 233 (1969).
[6] D. K. LILLY: *Phys. Fluids Suppl.*, **2**, 240 (1969).
[7] G. K. BATCHELOR: *J. Fluid Mech.*, **5**, 113 (1959).
[8] J. G. CHARNEY: *J. Atmos. Sci.*, **28**, 1087 (1971).
[9] P. B. RHINES: *The Sea*, Chap. VI (New York, N. Y., 1977), p. 189.
[10] R. SALMON: *Geophys. Astrophys. Fluid Dyn.*, **10**, 25 (1978).
[11] MODE GROUP: *Deep-Sea Res.*, **25**, 859 (1978).
[12] J. R. LUYTEN and J. C. SWALLOW: *Deep-Sea Res.*, **23**, 1005 (1976).
[13] C. WUNSCH: *J. Phys. Oceanogr.*, **7**, 497 (1977).
[14] E. HOPF: *J. Rat. Mech.*, **1**, 87 (1952).
[15] T. D. LEE: *Q. Appl. Math.*, **10**, 69 (1952).
[16] E. T. JAYNES: *Phys. Rev.*, **106**, 620 (1957).
[17] R. L. SELIGER and G. B. WHITHAM: *Proc. R. Soc. London Ser. A*, **305**, 1 (1968).
[18] A. I. KHINCHIN: *Mathematical Foundations of Information Theory* (New York, N. Y., 1957).

[19] R. SALMON, G. HOLLOWAY and M. C. HENDERSHOTT: *J. Fluid Mech.*, **75**, 691 (1976).
[20] G. HOLLOWAY: Ph. D. Dissertation, University of California San Diego (1976).
[21] N. P. FOFONOFF: *J. Mar. Res.*, **13**, 254 (1954).
[22] P. B. RHINES: *J. Fluid Mech.*, **69**, 417 (1975).
[23] P. B. RHINES: *Annu. Rev. Fluid Mech.*, **11**, 401 (1979).
[24] J. R. HERRING, S. A. ORSZAG, R. H. KRAICHNAN and D. C. FOX: *J. Fluid Mech.*, **66**, 417 (1974).
[25] S. A. ORSZAG: *J. Fluid Mech.*, **41**, 363 (1970).
[26] S. A. ORSZAG: *Fluid Dynamics*, edited by R. BALIAN and J. S. PEUBE (New York, N. Y., 1977).
[27] G. HOLLOWAY: *J. Fluid Mech.*, **82**, 747 (1977).
[28] R. H. KRAICHNAN: *J. Fluid Mech.*, **5**, 497 (1959).
[29] R. H. KRAICHNAN: *J. Fluid Mech.*, **47**, 513 (1971).
[30] R. H. KRAICHNAN: *J. Fluid Mech.*, **47**, 525 (1971).
[31] R. H. KRAICHNAN: *J. Atmos. Sci.*, **33**, 1521 (1976).
[32] C. E. LEITH: *J. Atmos. Sci.*, **28**, 145 (1971).
[33] C. E. LEITH and R. H. KRAICHNAN: *J. Atmos. Sci.*, **29**, 1041 (1972).
[34] J. R. HERRING: *J. Atmos. Sci.*, **32**, 2254 (1975).
[35] J. R. HERRING: *J. Atmos. Sci.*, **34**, 1731 (1977).
[36] G. HOLLOWAY: *J. Phys. Oceanogr.*, **8**, 414 (1978).
[37] J. R. HERRING: *J. Atmos. Sci.*, **37**, 969 (1980).
[38] R. SALMON: *Geophys. Astrophys. Fluid Dyn.*, **15**, 167 (1980).
[39] M. S. LONGUET-HIGGINS and A. E. GILL: *Proc. R. Soc. London Ser. A*, **299**, 120 (1967).
[40] K. HASSELMANN: *J. Fluid Mech.*, **30**, 737 (1967).
[41] G. P. WILLIAMS: *J. Atmos. Sci.*, **35**, 1399 (1978).